Piezoelectric Sensor/Actuator for Aeronautical Smart Structures Based on PVdF-CNTs Nanomembranes

Antonio Avila
Fundaçao de Desenvolvimento da Pesquisa - Fundep.

04/10/2019
Final Report

REPORT DOCUMENTATION PAGE

Form Approved
OMB No. 0704-0188

The public reporting burden for this collection of information is estimated to average 1 hour per response, including the time for reviewing instructions, searching existing data sources, gathering and maintaining the data needed, and completing and reviewing the collection of information. Send comments regarding this burden estimate or any other aspect of this collection of information, including suggestions for reducing the burden, to Department of Defense, Executive Services, Directorate (0704-0188). Respondents should be aware that notwithstanding any other provision of law, no person shall be subject to any penalty for failing to comply with a collection of information if it does not display a currently valid OMB control number.
PLEASE DO NOT RETURN YOUR FORM TO THE ABOVE ORGANIZATION.

1. REPORT DATE (DD-MM-YYYY) 10-04-2019	**2. REPORT TYPE** Final	**3. DATES COVERED** (From - To) 30 Sep 2014 to 31 Jan 2019

4. TITLE AND SUBTITLE Piezoelectric Sensor/Actuator for Aeronautical Smart Structures Based on PVdF-CNTs Nanomembranes	**5a. CONTRACT NUMBER**
	5b. GRANT NUMBER FA9550-14-1-0377
	5c. PROGRAM ELEMENT NUMBER 61102F
6. AUTHOR(S) Antonio Avila	**5d. PROJECT NUMBER**
	5e. TASK NUMBER
	5f. WORK UNIT NUMBER

7. PERFORMING ORGANIZATION NAME(S) AND ADDRESS(ES) Fundaçao de Desenvolvimento da Pesquisa - Fundep. Av. Antônio Carlos 6.627, - 4° andar Belo Horizonte, MG, 31270-901 BR	**8. PERFORMING ORGANIZATION REPORT NUMBER**

9. SPONSORING/MONITORING AGENCY NAME(S) AND ADDRESS(ES) AFOSR/SOARD U.S. Embassy Santiago Av. Andres Bello 2800 Santiago, Chile	**10. SPONSOR/MONITOR'S ACRONYM(S)** AFRL/AFOSR IOS
	11. SPONSOR/MONITOR'S REPORT NUMBER(S) AFRL-AFOSR-CL-TR-2019-0007

12. DISTRIBUTION/AVAILABILITY STATEMENT
A DISTRIBUTION UNLIMITED: PB Public Release

13. SUPPLEMENTARY NOTES

14. ABSTRACT
This report describes the activities developed during the Sept. 2014-January 2019 period. The project designed, synthetized/manufactured and optimized of sensors/actuators based on piezoelectric PVDF/CNT nanomembranes combined to shape memory alloys wires. The actuator was able to develop an angular deformation from 30 deg to 180 deg with an applied voltage of 30 V and 2 amps. The angular deformation response to applied voltage seems to be linear and gradual. The PVDF/CNT nanomembrane present a high piezoelectric activity with beta-phase formation reaching 94%. The sensors based on piezoelectric nanomembranes were able to generate voltages ranging from 2V to 12V.

15. SUBJECT TERMS
PVDF-HFP nanomembrane, Aeronautical Smart Structures, Piezoelectric Sensor, SOARD

16. SECURITY CLASSIFICATION OF:			**17. LIMITATION OF ABSTRACT**	**18. NUMBER OF PAGES**	**19a. NAME OF RESPONSIBLE PERSON** ANDERSEN, GEOFFREY
a. REPORT Unclassified	**b. ABSTRACT** Unclassified	**c. THIS PAGE** Unclassified	SAR		**19b. TELEPHONE NUMBER** (Include area code) 703-615-9465

Standard Form 298 (Rev. 8/98)
Prescribed by ANSI Std. Z39.18

FINAL REPORT

1. Project Identification:

Project Title: Piezoelectric Sensor/Actuator for Aeronautical Smart Structures Based on PVdF-CNTs Nanomembranes
Project Reference Number: FA9550-14-1-0377
Principal Investigator: Prof. Antonio Avila
Place: Universidade Federal de Minas Gerais - Brazil
Evaluation Time Frame: September 30, 2014 to January 31, 2019
Project Manager: Dr. James Fillerup (1st to 3rd years) Dr. Michael Martinez (4th year)

2. Abstract

This report describes the activities developed during the Sept. 2014-January 2019 period. The project designed, synthetized/manufactured and optimized of sensors/actuators based on piezoelectric PVDF/CNT nanomembranes combined to shape memory alloys wires. The actuator was able to develop an angular deformation from 30 deg to 180 deg with an applied voltage of 30 V and 2 amps. The angular deformation response to applied voltage seems to be linear and gradual. The PVDF/CNT nanomembrane present a high piezoelectric activity with beta-phase formation reaching 94%. The sensors based on piezoelectric nanomembranes were able to generate voltages ranging from 2V to 12V.

3. Important note:

There was a one year delay on the last year grant payment. Therefore, it was granted a 10 months extension without payment. This "extra" time was used to finish experiments and organize data.

4. Project milestones:

The first year was dedicated to the search for the best options for nanomembranes synthesis. This is a critical issue to the research project as the piezoelectric behavior is directly affected by the manufacturing parameters. These parameters are dependent of the type of polymer solution employed, and the manufacturing process selected. During the first year project the following milestones were achieved:

Milestone #1: Polymeric solution synthesis/selection;

- ✓ Piezoelectric polymers selected:
  - o Polyvinylidene fluoride (PVdF) – Imported from the US Sigma Aldrich (expected to arrive in Brazil by 02/2015);
  - o Polyvinylidene fluoride-co-trifluoroethylene *(PVdF-TrFE)* – Imported from France Arkema (arrived in Brazil by 12/19/2014);
  - o Polyvinylidene fluoride-co-hexafluoropropene (PVdF-HFP) – from Sigma Aldrich Brazil (10/13/2014);

- ✓ Piezoelectric polymers solution:
  - o Solvent: N,N dimethylformamide (DMF);
  - o Concentrations: The DMF/PVdF ratio ranged from 93/7 to 86/14 in weight percentage.

✓ Nanomembranes synthesis:

    o   Process: Electrospinning (see figure 1)

The electrospinning parameters selected as the ones which have direct influence on nanomembranes morphology and consequently to the piezoelectric response were gap between needle tip and cylinder (target), applied voltage, solution concentration (ratio between polymer/solvent), and solution flow rate. The piezoelectric activity is based on the beta phase formation. Moreover, the beta phase formation is induced by the polymer deformation by stretching. The set of experiments were designed in such a way that the best possible nanomembrane was synthetized. There are many different ways to stretch nanofibers. One is to decrease the solution flow, which can lead to very thin fibers and consequently to fragile. Another option is to increase the applied voltage, which increase the fiber driving force, but a high voltage can bring as a problem of spark formation and nanomembrane damage. The increase of gap could be another strategy employed, but a large distance will require a large applied electric power to initiate the electrospinning process. Based on these comments and the series of experiments were performed and the near optimal parameters obtained were:

✓ Gap needle tip- cylinder (target) ≈ 6 in (150 mm);

✓ Voltage applied: 20 KV;

✓ Solution concentration: DMF/PVdF-HFP: 86/14;

✓ Flow rate: 0.001 liter/hour (2.65×10^{-4} gallons/hour);

✓ Substrate: aluminum foil

Figure 1: Electrospinning device at UFMG's laboratory

The nanomembrane obtained using these parameters are homogeneous, easy to remove from the aluminum substrate and flexible, as shown in Figures 2A-2B.
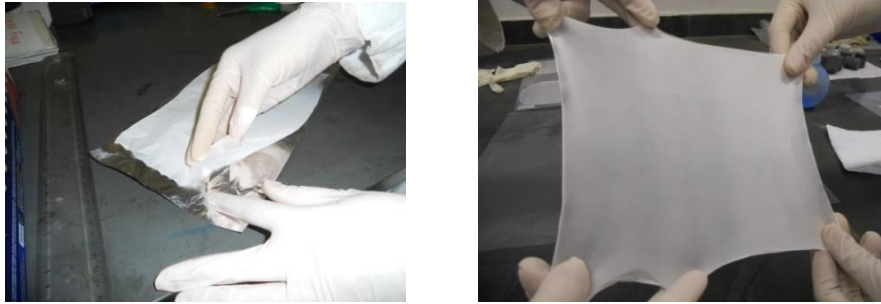
Figure 2. Nanomembranes prepared using the electrospinning parameters

An important issue for development of a sensor/actuator based on piezoelectric nanomembranes is the nanomembranes' characterization. At this level of characterization the focused was on nanomembranes' morphology. It is important to mention that the membranes' morphology has direct influence into the piezoelectric activity due to the amount of stretching applied to each individual fibers. This analysis was done using two standard techniques, i.e. scanning electronic microscopy and atomic force microscopy.

Milestone #2: Nanomembranes characterization:

- ✓ Atomic force microscopy (AFM) and high resolution scanning electron microscopy (HRSEM);

Figure 3 AFM/3D representation of a nanomembrane made of PVDF-HFP and doped with carbon nanotubes (0.3 wt. %). A carbon nanotube cluster formation (≈ 200 nm) was observed. The idea behind dope the PVDF nanomembrane with carbon nanotube was to improve the piezoelectric activity and at same time create a path to electric current generated during the piezoelectric activity. The cluster formation indicated that different dispersion processes should be investigate in order to have a more homogeneous carbon nanotube distribution.
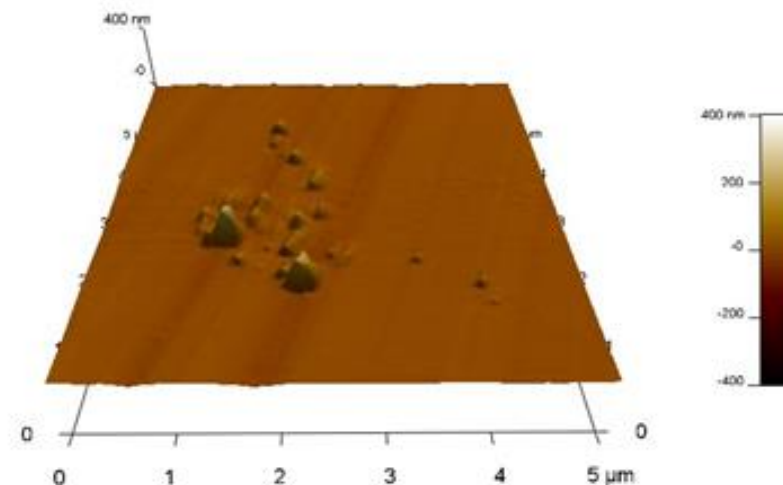

Figure 3: AFM observation

The high resolution scanning microscopy (HRSEM) was employed to investigate not only the fibers' morphology but it was also used to observe the interaction between the aluminum substrate and the fibers.

Figure 4 shows a HRSEM of a PVDF-HFP nanomembrane and the fibers' diameter size distribution. The dimensions can be classified as sub-micron dimensions (average diameter around 562 nm), and the standard deviation also indicates a reasonable size distribution. Note that the fiber size distribution is not a Gaussian distribution, which was expected due to solvent evaporation.
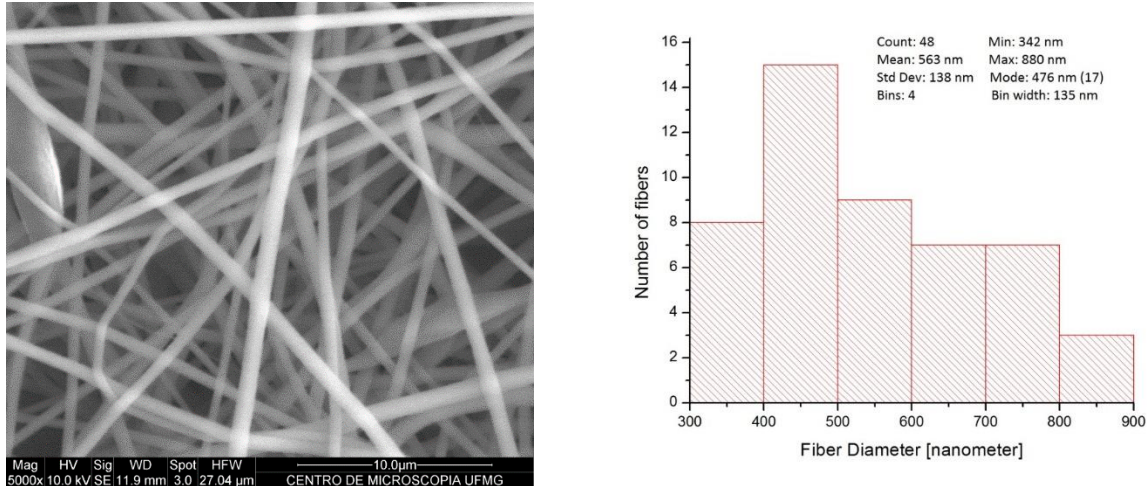

Figure 4: HRSEM Observation

An important issue during the nanomembranes' manufacturing is its adhesion to the substrate. A strong adhesion to the substrate can cause damage during the membrane's removal. Figure 5 shows the formation of an interface between the aluminum sheet and the nanomembrane (it is the white formation close to the aluminum surface). This interface had a twofold role, the first one is to form a base for the nanomembrane growth and the second one is to allow the nanomembrane to detach from the substrate.
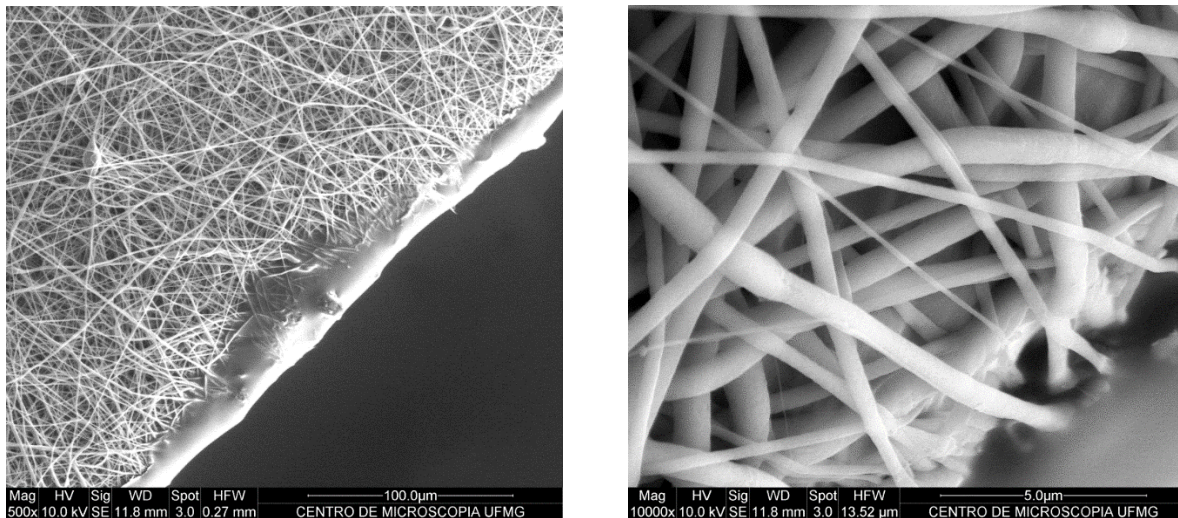
Figure 5: HRSEM – Interface substrate/nanomembrane

During the second year project the following milestones were achieved:

- ✓ Polymeric solution synthesis and nanostructure dispersion;
  - o MWNT and/or Nickel chloride hexa-hydrate.
- ✓ Nanomembranes synthesis;
  - o Searching for the highest beta phase formation configuration;
- ✓ Nanomembranes characterization;
  - o SEM, AFM, TEM, FTIR, raman spectroscopy;
- ✓ Design of actuator/sensor:
  - o Actuator - proof of concept;

To be able to understand each milestone achieve, it is important to describe each of them. The first step was the polymeric solution preparation to electrospinning the nanomembrane. Let open a "parenthesis" to explain what the electrospinning process is. The electrospinning is a technique employed to create small diameter fibers by electrical discharge, in general high voltage (between 10 to 30 KV). The technical parameters employed for the electrospinning process (best results obtained) can be described as follows:
- ✓ Gap needle tip- cylinder (target) ≈ 6 in (150 mm);
- ✓ Voltage applied: 20 KV;
- ✓ Solution concentration: DMF/PVdF-HFP: 86/14;
- ✓ Flow rate: 0.001 liter/hour (2.65×10^{-4} gallons/hour);
- ✓ Substrate: aluminum foil

Note that as this research deals with piezoelectricity, different PVdF co-polymers was tested. In this case, the tested co-polymers were:
- ✓ Piezoelectric polymers selected:
  - ✓ Polyvinylidene fluoride-co-hexafluoropropene (PVdF-HFP) – from Sigma Aldrich Brazil ;
  - ✓ Polyvinylidene fluoride (PVdF) – Imported from the US Sigma Aldrich;
  - ✓ Polyvinylidene fluoride-co-trifluoroethylene (PVdF-TrFE) – Imported from France Arkema;
- ✓ Piezoelectric polymers solution:
  - ✓ Solvent: N,N dimethylformamide (DMF);
  - ✓ Concentrations: The DMF/PVdF ratio ranged from 80/20 to 85/15 percentage, in weight.
  - ✓ Dispersion method: Ultrasonication @ 42 KHz

The reason to use different co-polymers is due to the amount of beta phase formed by each combination. The beta phase formation is the phase responsible to the piezoelectric behavior. To be able to increase even more the piezoelectric response, carbon based nanostructures, i.e. carbon nanotubes and graphene, were dispersed to the polymeric solution. The nanostructures and/or nanoparticles employed in this research are:

- ✓ Graphene (Multi-layer graphene ~ 12 layers of graphene);
- ✓ Carbon nanotubes (Multi-walled carbon nanotubes);
- ✓ Nickel chloride hexa-hydrate;

Figures 6A-B show the graphene type nanostructure prepared inside the Mechanics of Nanostructures Laboratory (Professor's Avila lab). Note that, in Figure 3B, there is an interaction between the carbon nanotube (CNT) and the graphene.

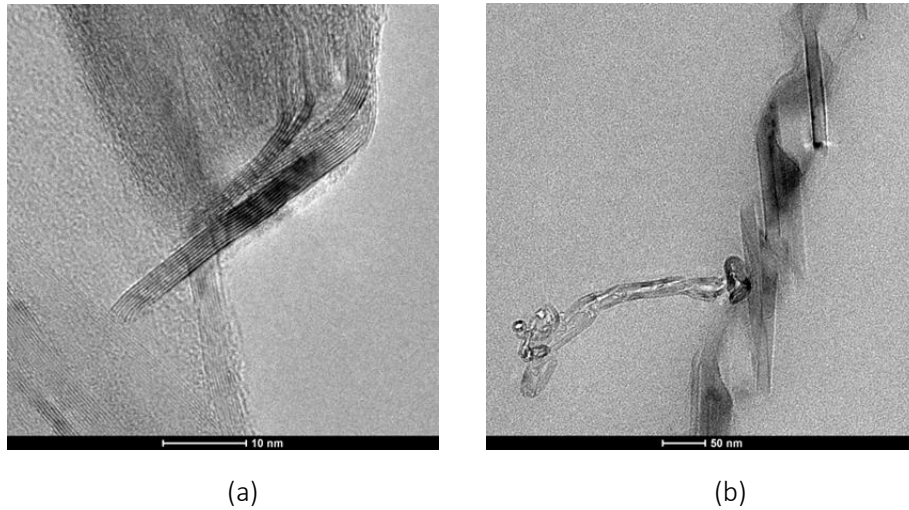(a)   (b)

Figure 6: Carbon based nanostructures. (a) Graphene; (b) Carbon nanotubes + graphene

The carbon based nanostructure morphology can be evaluated using Atomic Force Microscopy (AFM). These nanostructures inside the nanofibers will affect not only the fibers formation but its piezoelectric response. Figures 7A-B show the graphene and carbon nanotubes nanostructures formed inside the nanofibers. The graphene nanostructures are more concentrated while the CNTs are dispersed into the polymeric nanofibers.

(a)
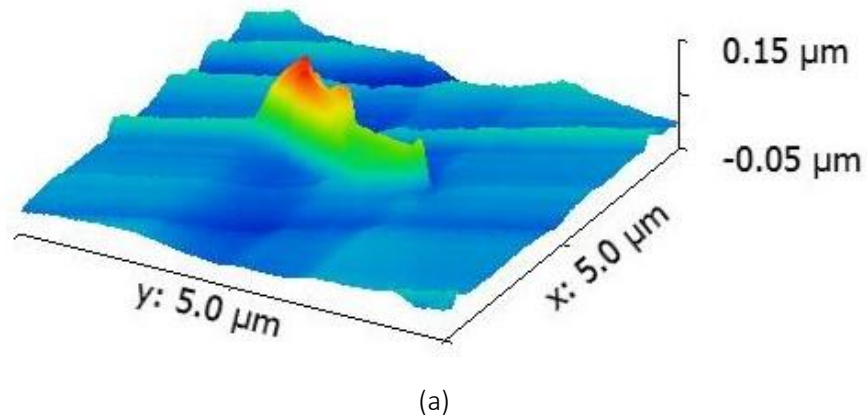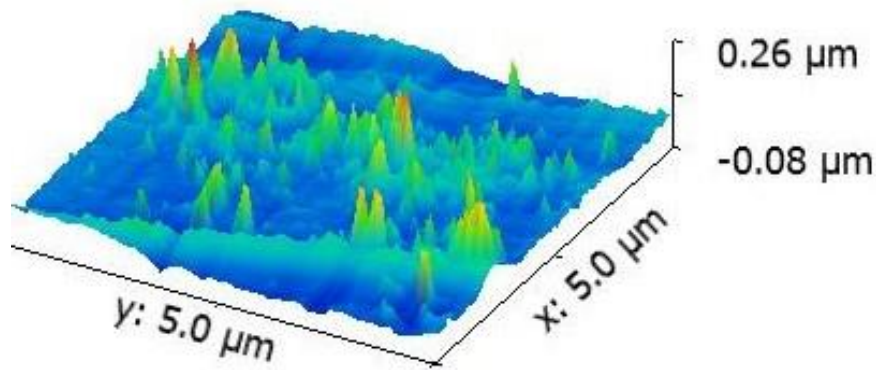
(b)

Figure 7: AFM Observations; (a) Graphene; (b) CNTs

The strategy employed to search for the highest beta phase formation can be described by the flow chart represented in Figure 8.
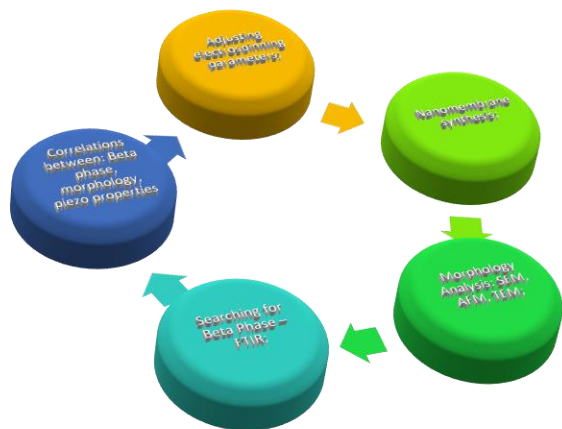
Figure 8: Flow chart for searching for the best beta phase formation configuration

To be able to implement this search a design of experiment matrix was developed. This matrix of experiments is based on the following parameters:

- ✓ Three different polymers (PVDF, PVDF-HFP, PVDF-TrFe);
- ✓ Four Electrospinning parameters (gap, applied voltage, polymer/solvent concentration, solution flow rate);
- ✓ Two different nanostructures (CNT, Nickel);
- ✓ Three different nanostructures concentrations;
- ✓ Two types of CNT functionalization: SDBS and No-SDBS

Based on those parameters the total number of experiments was 864. At the AFOSR meeting in Ohio, July 2016, it was clear that this amount of experiments is too large. Therefore, by making some quantities fixed (mostly the electrospinning parameters: gap, applied voltage, flow rate and solution/solvent ratio) the total

amount of experiments (nanomembranes prepared) was reduced to 63. This amount of nanomembranes is more feasible number to be tested. From the 2015-2016 year these are the following results:

- ✓ **Group #1:** PVDF-HFP

Table 1 summarizes the tests performed using the same electrospinning parameters described previously.

Table 1. Group 1 Main parameters summary

Sub-group ID	Polymer Concentration [%]	CNT [wt.%]	Solvent	Functionalization: Surfactant
A1	14	----	DMF	----
A2	14	0.60	DMF	----
A3	14	0.15	DMF	SDBS
A4	14	0.30	DMF	SDBS
A5	14	0.30	DMF	----
A6	14	0.60	DMF	SDBS
A7	14	0.15	DMF	----

Figures 9A-B show the fibers dispersion/morphology and the size distribution considering 50 measurements for sub-group A1.
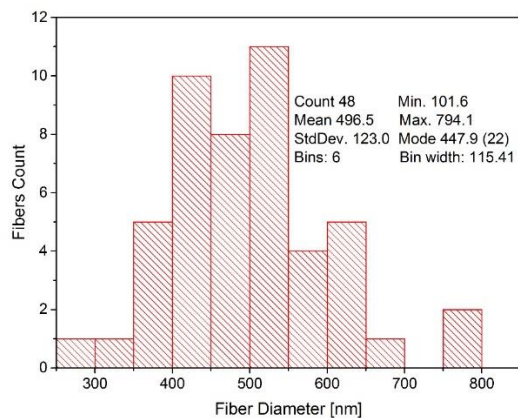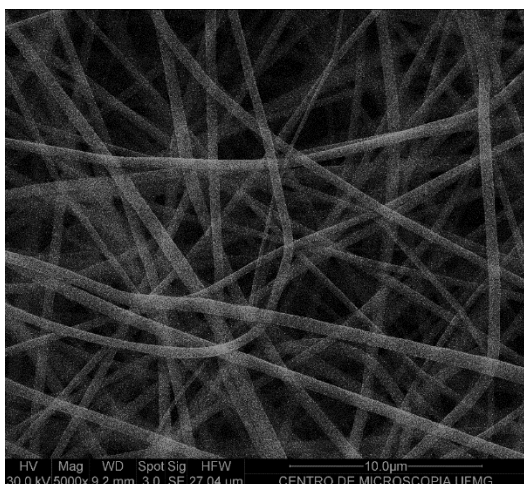
(a)

(b)

Figure 9: Sub-group A1. (a) SEM observation. (b) Fibres distribution

As it can be observed the nanofibers average diameter is a sub-micro diameter, around 500 nm. The fibers distribution is close to a normal distribution. The Fourier Transform Infra-Red (FTIR) analysis for sub-group A1 is shown in Figure 10.
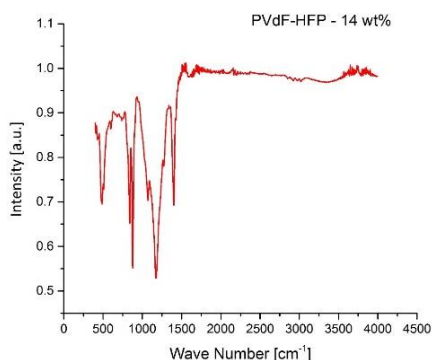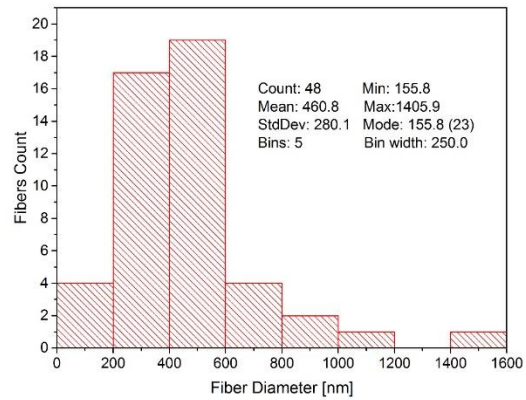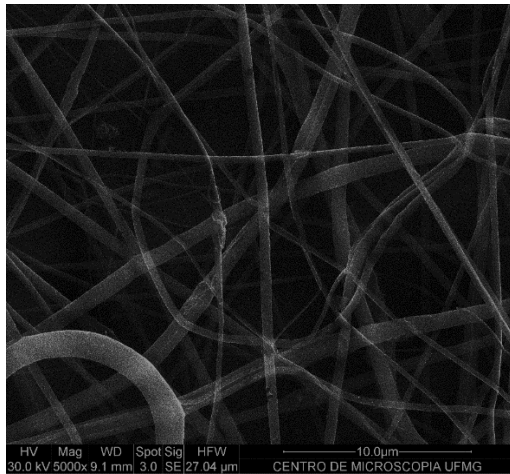

Figure 10: FTIR signature for sub-group A1

The FTIR analysis can be translated by the following wave numbers: **Beta phase:** 509(bending), 839(rocking), 877(rocking + stretching), 1073 (wagging), 1175(bending), 1275(stretching + bending), 1400(wagging), 1430 (bending). **Amorphous phase:** 488 and 600. The information between brackets are the vibration modes correspondent to the wave number.

Figures 11A-B show the SEM observation and the fibers' diameter distribution for the A2 sub-group. Note that in this case, the average diameter is around 10% smaller, but the standard deviation is higher. This indicates a larger variation on diameters. The FTIR signature (Figure 12) points to formation of alpha phase in addition to the beta and amorphous phases spotted in the previous samples. The FTIR analysis can be translated by the following wave numbers: **Beta phase:** 441(rocking), 508(bending), 839 (rocking + stretching), 876 (stretching + wagging), 1072 (stretching + wagging), 1175 (bending), 1275 (stretching + bending), 1400 (wagging + stretching), 1429 (bending). **Amorphous phase:** 486 and 599. **Alpha phase:** 762(bending).

<center>(a)</center>

<center>(b)</center>

<center>Figure 11: Sub-group A2. (a) SEM observation. (b) Fibres distribution</center>
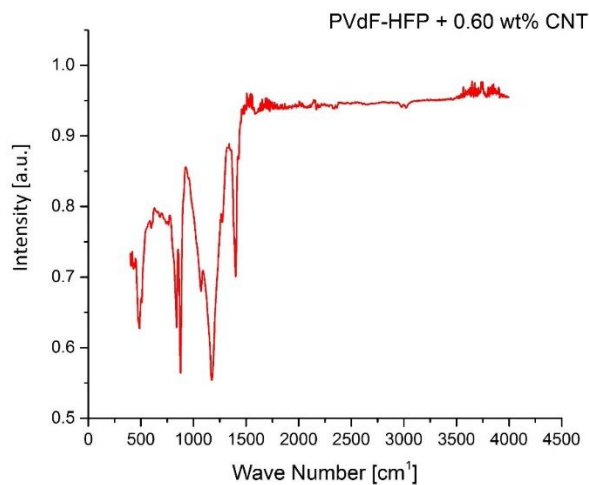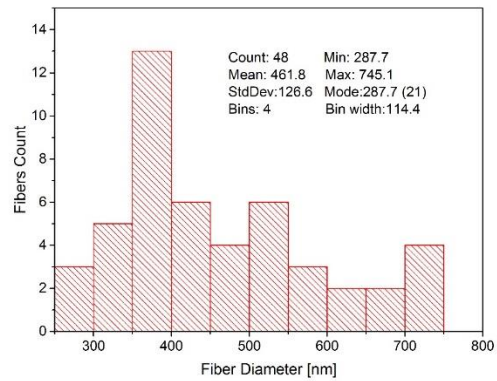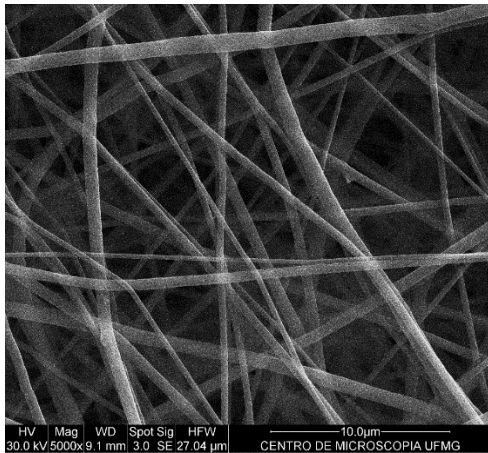

<center>Figure 12: FTIR signature for A2 subgroup</center>

Figures 13A-B show the SEM observation and the fibers' diameter distribution for the A3 sub-group. Note that in this case, the average diameter is around 462 nm, with a small standard deviation. This indicates a small variation on diameters. The FTIR signature (Figure 11) points to formation of alpha phase in addition to the beta and amorphous phases spotted in the previous samples. The FTIR analysis can be translated by the following wave numbers: **Beta phase:** 442 (rocking), 509 (bending), 839 (rocking + stretching), 877 (stretching), 1072 (stretching + wagging), 1175(bending), 1275(stretching + bending), 1400 (wagging + stretching), 1430 (bending). **Amorphous phase:** 487 and 601. **Alpha phase:** 410(rocking).

(a)   (b)

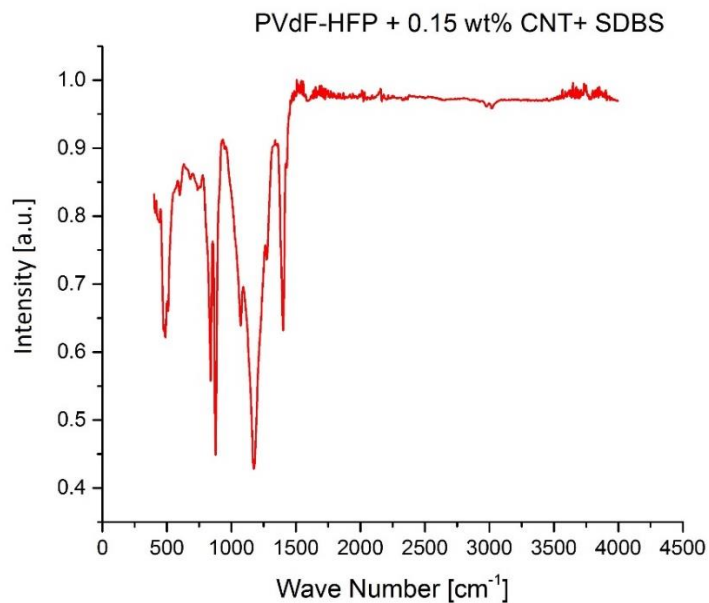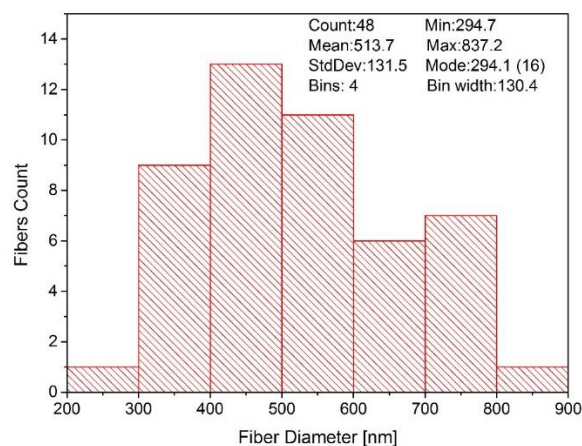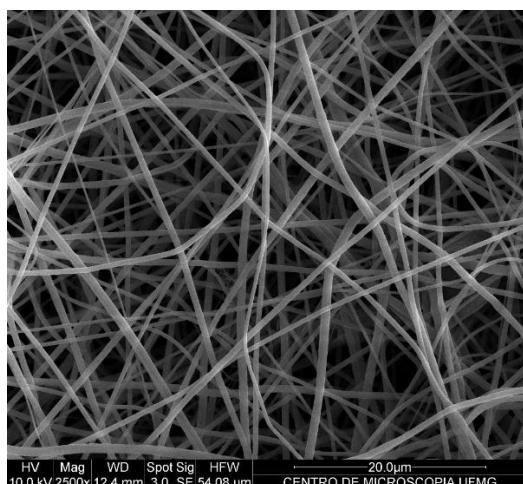Figure 13: Sub-group A2. (a) SEM observation. (b) Fibres size distribution

Figure 14 FTIR signature for A3 subgroup

Figures 15A-B show the SEM observation and the fibers' diameter distribution for the A4 sub-group. Note that in this case, the average diameter is around 514 nm, with a small standard deviation. This indicates a much more homogeneous fibres distribution. The FTIR signature (Figure 14) points to formation of alpha phase in addition to the beta and amorphous phases spotted in the previous samples. The FTIR analysis can be translated by the following wave numbers: **Beta Phase:** 442 (rocking); 509 (bending); 839 (stretching + rocking); 877 (stretching); 1072 (wagging); 1175(bending); 1275 (stretching + bending); 1400 (wagging + stretching); 1430 (bending). **Amorphous phase:** 486 and 601; **Alpha phase:** 762 (bending).

(a)   (b)

Figure 15: Sub-group A4. (a) SEM observation. (b) Fibres size distribution
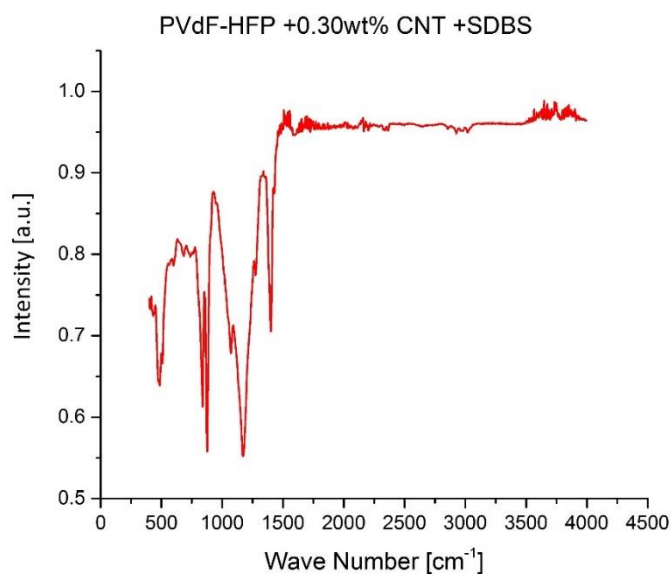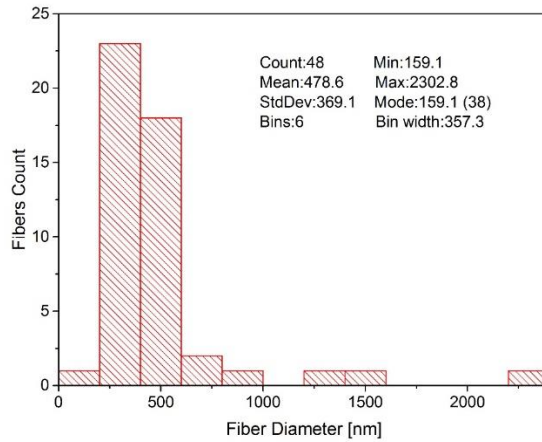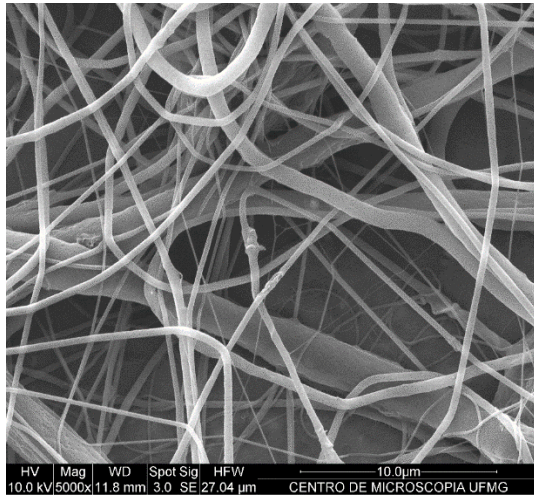

Figure 16 FTIR signature for A4 subgroup

Figures 17A-B show the SEM observation and the fibers' diameter distribution for the A5 sub-group. Note that in this case, the average diameter is around 480 nm, with large standard deviation. This indicates a huge difference between fibre diameters, and therefore a non-homogeneous fibres distribution. The FTIR signature (Figure 16) points to formation of alpha phase in addition to the beta and amorphous phases spotted in the previous samples. The FTIR analysis can be translated by the following wave numbers: **Beta Phase:** 441 (rocking); 508 (bending); 839 (rocking + bending); 877 (wagging + stretching); 1072 (stretching + wagging); 1177 (bending); 1274 (stretching + bending); 1400 (wagging + stretching); **Amorphous phase:** 486; **Alpha phase:** 407 (rocking); 612 (bending); 761(bending).

(a)   (b)

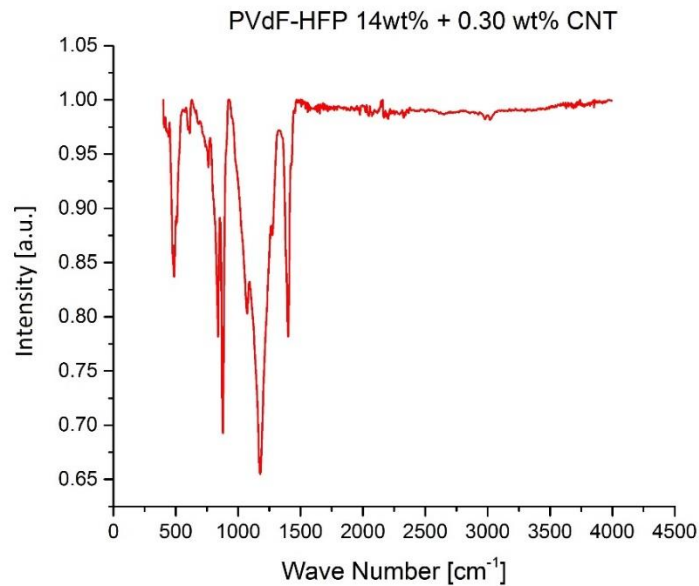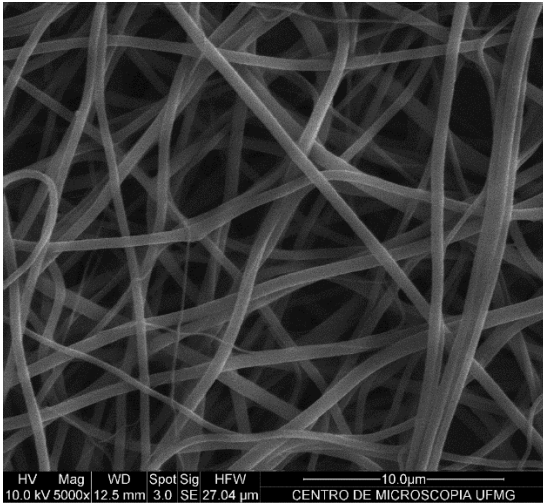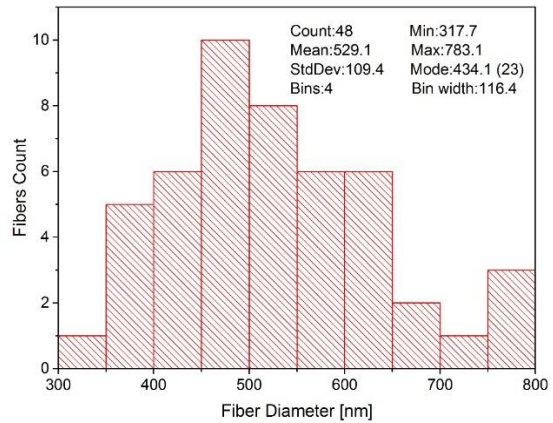Figure 17: Sub-group A5. (a) SEM observation. (b) Fibres size distribution

Figure 18 FTIR signature for A5 subgroup

Figures 19 A-B show the SEM observation and the fibers' diameter distribution for the A6 sub-group. Note that in this case, the average diameter is around 529 nm, a standard deviation around 110 nm. This indicates a fair size difference between fibre diameters, and therefore a quasi-homogeneous fibres distribution. The FTIR signature (Figure 18) points to formation of beta phase in addition to amorphous phase spotted. The FTIR analysis can be translated by the following wave numbers: **Beta Phase:** 441 (rocking); 509 (bending); 839 (rocking + bending); 878 (wagging + stretching); 1073 (stretching + wagging); 1177 (bending); 1274 (stretching + bending); 1401 (wagging + stretching); 1430 (bending). **Amorphous phase:** 486 and 600; No alpha phase was detected in this case.

(a)   (b)

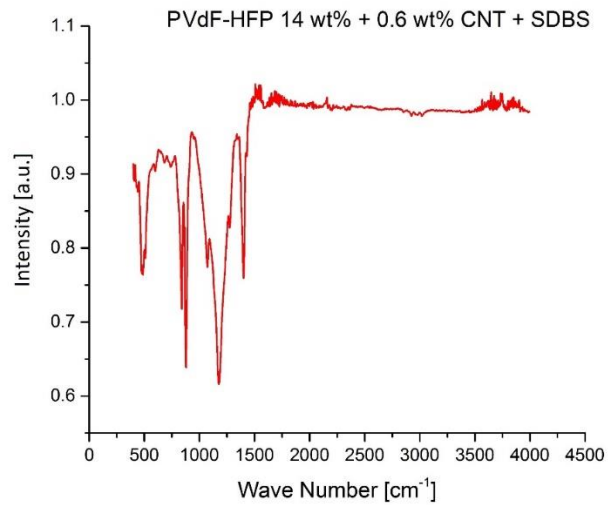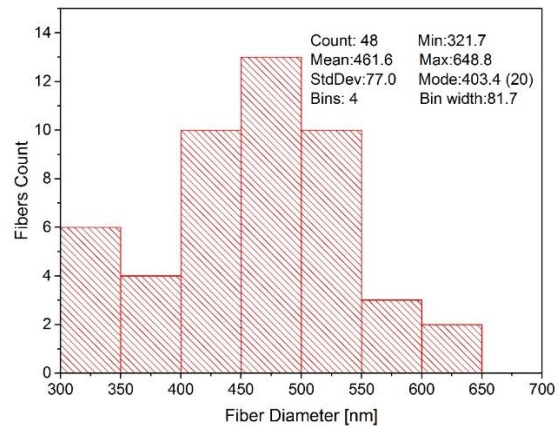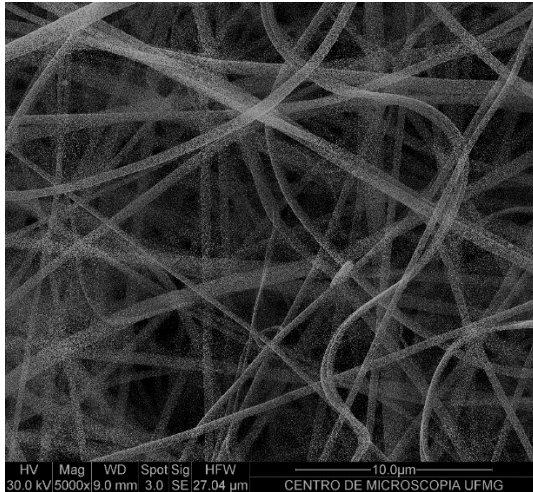Figure 19: Sub-group A6. (a) SEM observation. (b) Fibres size distribution

Figure 20: FTIR signature for sub-group A6

The addition of functionalized carbon nanotube lead to a quasi-homogeneous fiber morphology and no alpha phase formation. Figures 21 A-B show the SEM observation and the fibers' diameter distribution for the A7 sub-group. Note that in this case, the average diameter is around 461 nm, a standard deviation around 77 nm. This indicates a small size difference between fibre diameters, and therefore a near quasi-homogeneous fibres distribution. The FTIR signature (Figure 20) points to formation of alpha and beta phase in addition to amorphous phase spotted. The FTIR analysis can be translated by the following wave numbers: **Beta Phase:** 441 (rocking); 509 (bending); 836 (rocking + bending); 876 (wagging + stretching); 1072 (stretching + wagging); 1178 (bending); 1275 (stretching + bending); 1401 (wagging + stretching). **Amorphous phase:** 487; Alpha phase: **phase:** 410 (rocking); 612 (bending); 761 (bending);

<center>(a)   (b)</center>

<center>Figure 21: Sub-group A7. (a) SEM observation. (b) Fibres size distribution</center>

<center>Figure 22: FTIR signature for sub-group A7</center>
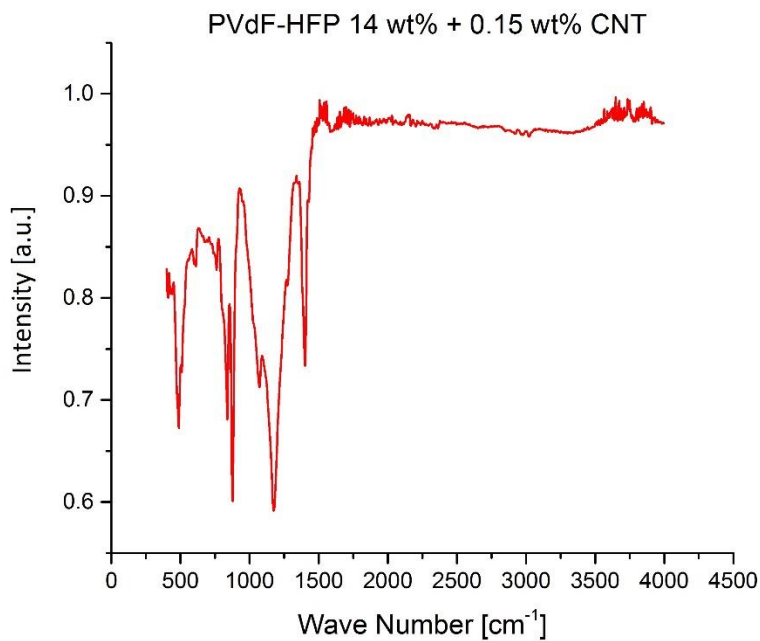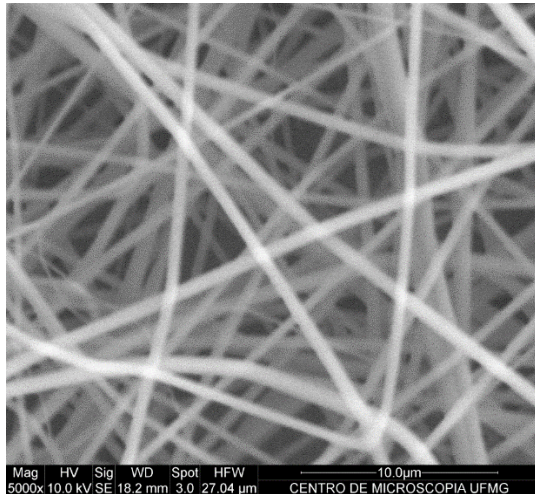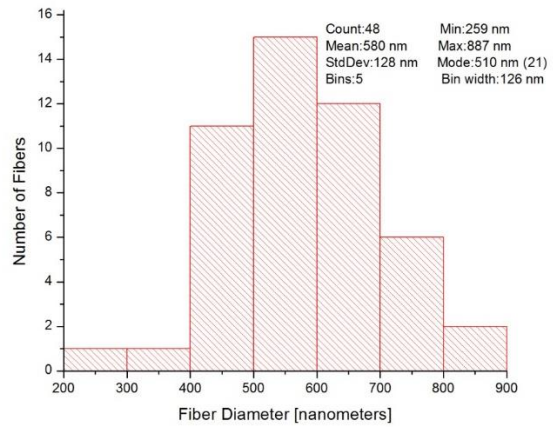
✓ **Group #2:** PVdF:

For conciseness, only the first sub-group of group #2 is shown. Figures 23A-B show the fibers' morphology and the fibers' size distribution. As it can be observed the average diameter size is around 560 nm, a sub-micron class. Moreover, the standard deviation is around 130 nm, which is a fair size and leads to a quasi-homogeneous distribution.

Figure 23: Group 2. (a) SEM observation. (b) Fibres size distribution

✓ **Group #3:** PVdF-TrFe:

Figure 24A-B represent the fibers morphology and the fiber diameter distribution. The average fiber size was around 466 nm with a much larger standard deviation.
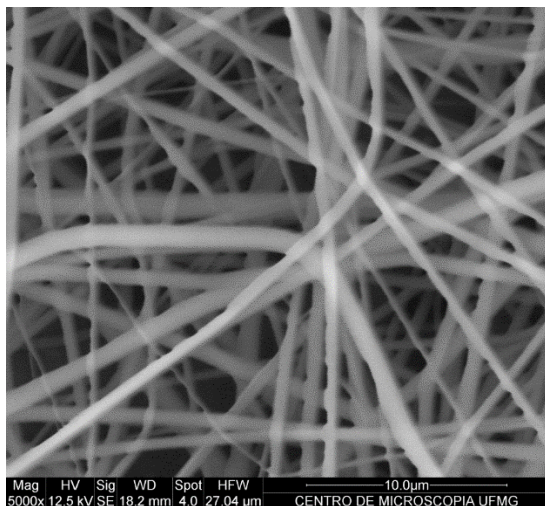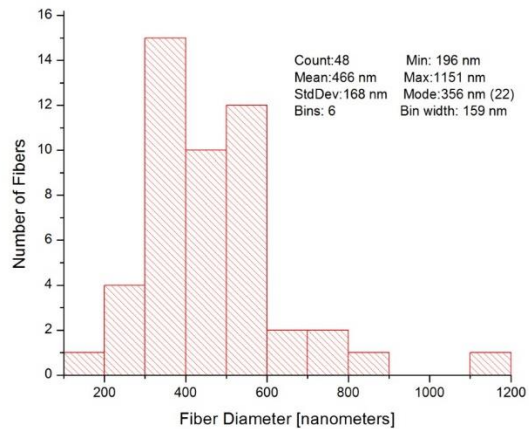
(a)   (b)

Figure 24: Group 3. (a) SEM observation. (b) Fibres size distribution

✓ Piezoelectric behavior using FTIR information:

As it can be noticed the polymeric chains are slightly different. Note all electrospinning parameters were the same for all groups, but the morphology varies. Therefore, some comments can be made:

✓ CNTs : changes on morphology

✓ Beta phase formation : CNTs concentration and surfactant

How quantity the beta phase formation?

✓ From literature, we have: $F(\beta) = \dfrac{A_\beta}{1.26A_\alpha + A_\beta}$

were A = absorbance: for alpha @ 764 cm-1 and 840 cm-1 for beta

Table 2 summarizes the data obtained for all three groups. Notice that the subgroups in bold are the ones with the highest beta phase formation. As it can be observed, the CNT addition with and without functionalization lead to the best results. However, the three subgroups, #4, #17 and #19 are statistically identical, but there is a large difference when price is considered. The PVDF-TrFe co-polymer has a cost of € 7.00/gram, while the PVDF-HFP the cost is around US$ 0.45/gram+ SDBS: ¢ 0.026/gram. The best option is the PVDF-HFP + CNT+SDBS. The cost is low and the amount of beta phase is high.

Table 2: FTIR – Beta phase formation

Sample ID	Sample Composition	Beta Phase [%]
1	PVDF-HFP	78.8
2	PVDF-HFP+0.6CNT	58.7
3	PVDF-HFP+0.15CNT+SDBS	76.4
4	**PVDF-HFP+0.30CNT+SDBS**	**99.4**
5	PVDF-HFP+0.3CNT	57.0
6	PVDF-HFP+0.60CNT+SDBS	92.0
7	PVDF-HFP+0.15CNT	65.7
8	PVDF	76.8
9	PVDF+0.30CNT	66.3
10	PVDF+0.10Ni	61.9
11	PVDF+Ni+CNT	73.9

12	PVDF-HFP	75.2
13	PVDF-HFP+0.30CNT	59.9
14	PVDF-HFP+0.10Ni	72.9
15	PVDF-HFP+Ni+CNT	72.6
16	PVDF-TrFe	84.2
17	**PVDF-TrFe+0.30CNT**	**97.9**
18	PVDF-TrFe+0.10Ni	79.2
19	**PVDF-TrFe+Ni+CNT**	**98.8**

✓ *Sensor/actuator design:*

The idea is to design a sensor/actuator similar to the Micro Fibers Composites using the nanomembranes and MWNT/metal substrates. However, in small scale and associated in series and/or parallel. See illustrative figure from Kruusamae et al. (2015)[1]. (see Figures 22A-B
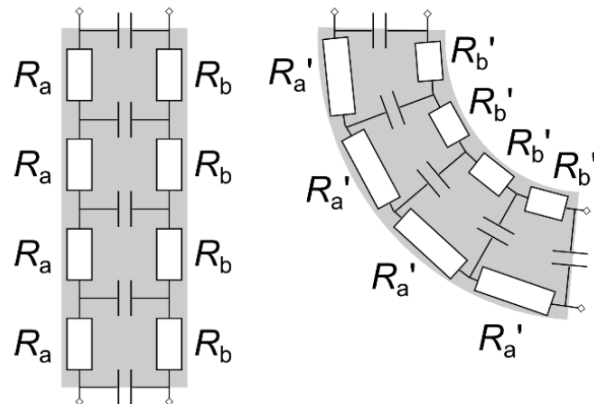

Figure 25. Sensor/actuator design (a): before bending; (b) after bending.

---

[1] Kruusmae et al., Actuators, 2015, 17-38; doi:10.3390/act4010017

A combination of SMA and Nanofibers was selected. Moreover, the SMAs are placed inside the nanomembranes layers.

NOTE: a small video with the proof of concept of this design was shown in the Ohio meeting in JJuly 2016

The activities during the third and fourth year were reduced due to 13 months delay on second year payment. The activities, however, focused on two major areas, i.e. the optimization of nanomembranes synthesis and the design and fabrication of a sensor/actuator.

## Optimization of nanomembrane synthesis:

The nanomembranes prepared during the second year could be divided in three groups:

- ✓ Polyvinylidene fluoride (PVdF) ;
- ✓ Polyvinylidene fluoride-co-hexa-fluoro-propene (PVdF-HFP) ;
- ✓ Polyvinylidene fluoride-co-trifluoroethylene (PVdF-TrFE)

The electrospinning parameter employed were detailed at the second year report and it will not be reproduced in this report. However, some important points regarding the nanomembranes' morphology. Note that changes on morphology can affect the nanomembranes' piezoelectric response.

Figures 26A-B show two nanomembranes, i.e. one made of PVDF and another one made of PVDF-HFP. In both cases, it is possible to observe formation of beads, small in-homogeneities associated to the fibers' formation. To be able to have a high piezoelectric response, the PVDF's crystalline phase has to be change from α phase to β phase. This is possible when   the PVDF membranes are stretched and large deformations are induced. In general, these deformations are around 300-600%. This is possible using electrospinning, when nanofibers were formed they are stretched, but when bead is formed a portion of PVDF solution solidifies without large deformations. This phenomenon lead to a decrease on overall β phase, and a decrease on piezoelectric activity.

The electrospinning parameters were reviewed and a hypothesis was formulated. Beads had an ellipsoidal shape and they are dispersed into the entire nanomembrane. The ellipsoidal shape could indicate a variation on   polymeric solution (PVDF/DMF-Acetone) flow rate close to the needle's wall. This variation can be represented by changes on shear forces near the needle's wall due to difference of evaporation rates of DMF and Acetone. The proposed solution involved two different approaches. The first one was to change the DMF/Acetone ratio from 80/20 to 50/50, and the second approach was to increase the needle diameter size from 25G (0.02025") to 18G (0.05"). The second approach lead to better results. As it can be seen in Figures 27A-B, the change on needle's diameter lead to a bead free nanomembrane for PVDF but a near-bead free for PVDF-HFP. By changing the both needle's diameter and the PVDF/Acetone ratio, the bead free PVDF-HFP nanomembrane was obtained (see Figure 28).
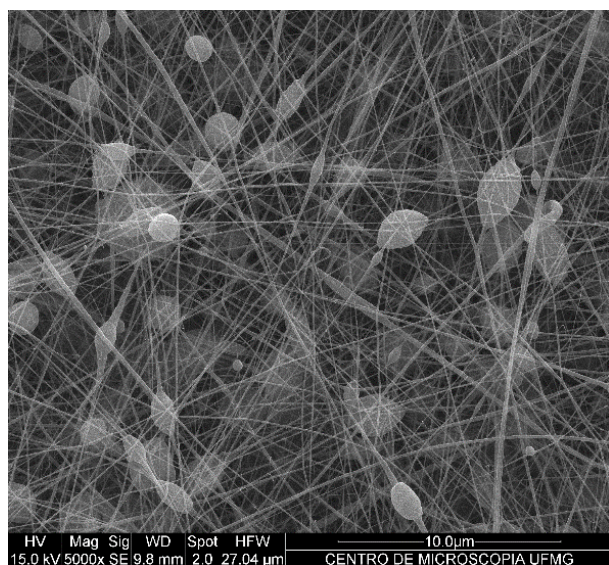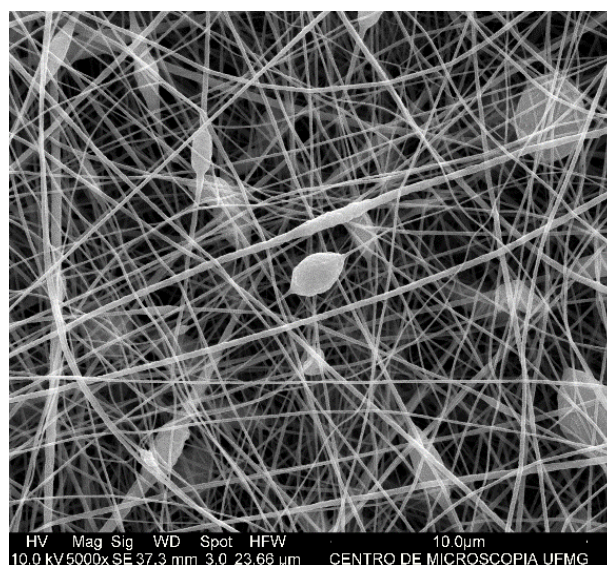
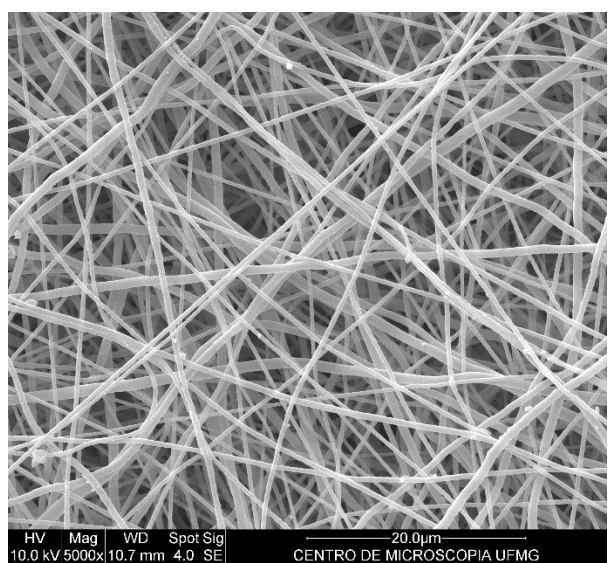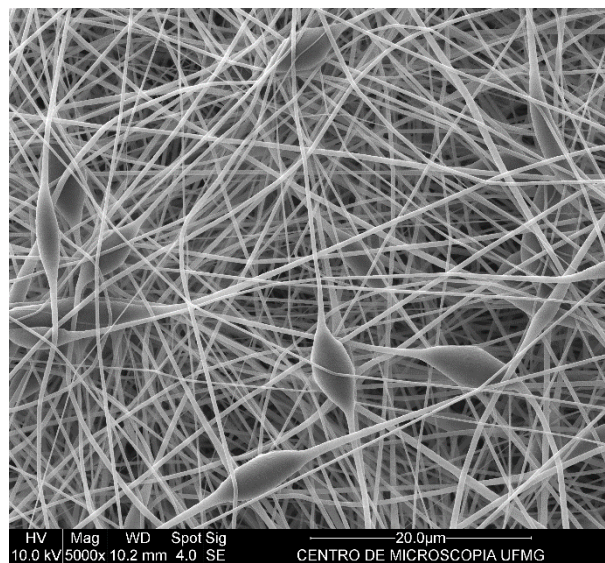(a)   (b)

Figure 26: Nanomembranes with beads. (a) PVDF nanomembrane; (b) PVDF-HFP nanomembrane

(a)   (b)

Figure 27: Nanomembranes. (a) PVDF nanomembrane; (b) PVDF-HFP nanomembrane near-bead free

The PVDF-TrFE nanomembranes did not presented bead formation during the second year synthesis. To be able to keep a fair comparison between all groups, a new set of PVDF-TrFE nanomembranes were synthetized using the same needle and DMF/acetone ratio used for the PVDF and PVDF-HFP ones. As it can be noticed in Figures 29A-B some morphological changes were observed. These changes were expected as the shear forces inside the polymeric solution changes.
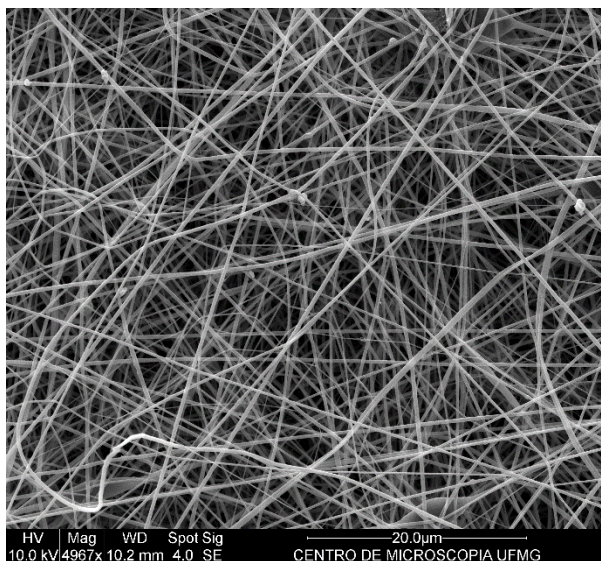
Figure 28. PVDF-HFP bead-free nanomembrane
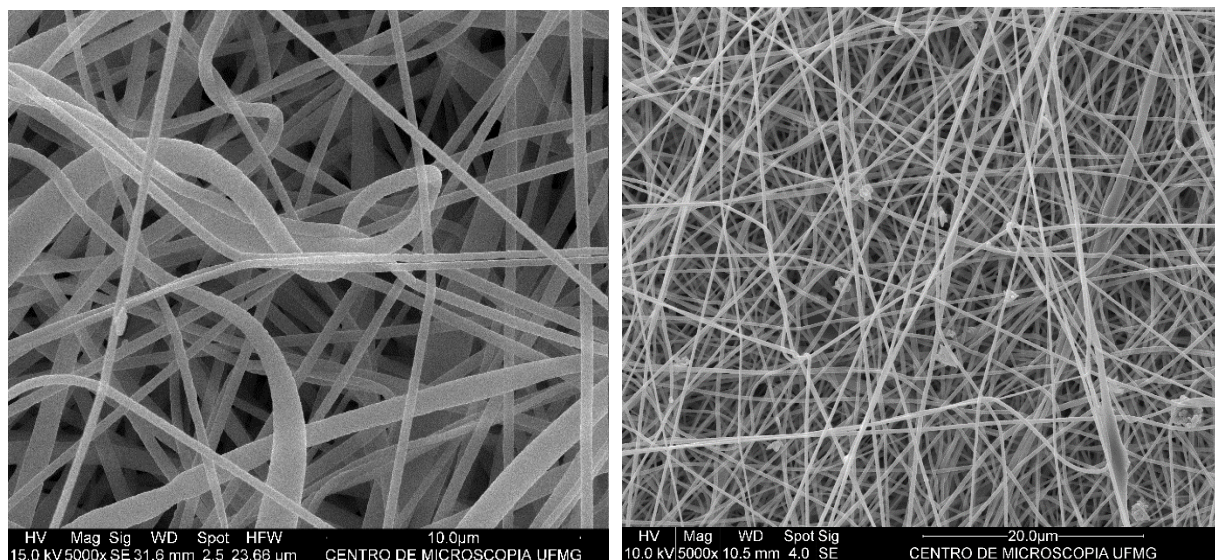
| (a) | (b) |

Figure 29. PVDF-TrFE nanomembranes; (a) 2nd year synthesis; (b) 3rd year synthesis

Changes on morphology can be described by two main factors: fibers' diameter and spatial distribution. Figures 30A-B describe the fibers' diameter distribution and mean values. Diameters were reduced, in average, by a factor of 1.86. It means that the new diameter was reduced to 46.23% of the original diameter. This drastically reduction of diameter lead to an increase on piezoelectric activity as it can be observed in Fig. 31A-B the FTIR spectra. Notice that by decreasing fibers' diameter, the fibers' deformation by stretching increased and the β phase formation was increased.

Count:50   Skewness:0.43   Weibull fit
Mean:401.28 Median:409.42 Mode:437.92
1st Quartile:305.45   3rd Quartile:460.99

Count:50 Skewness:0.37 Lognormal
Mean:185.54 Median:175 Mode:160
1st Quartile:160   3rd Quartile:215

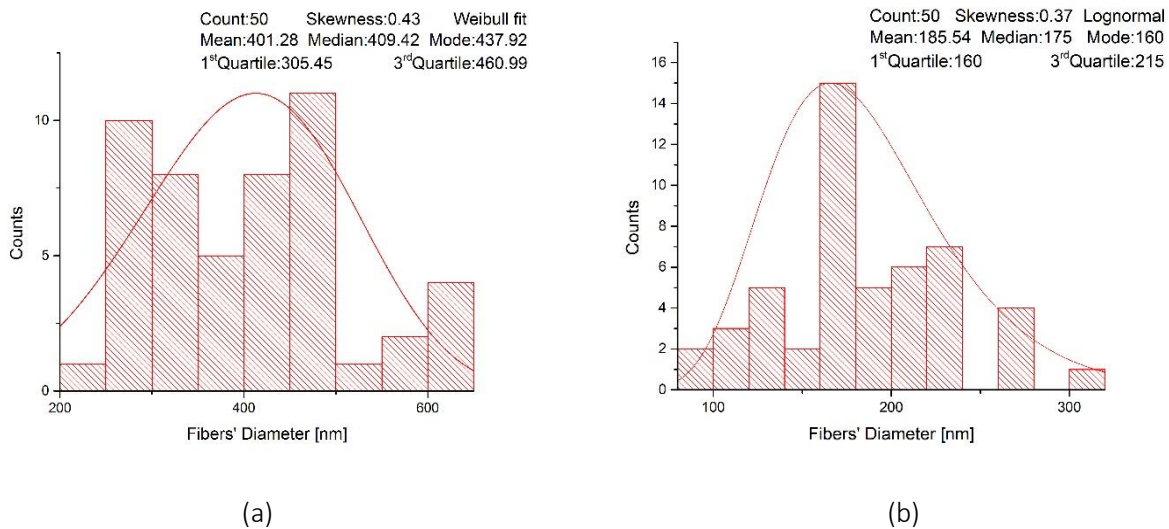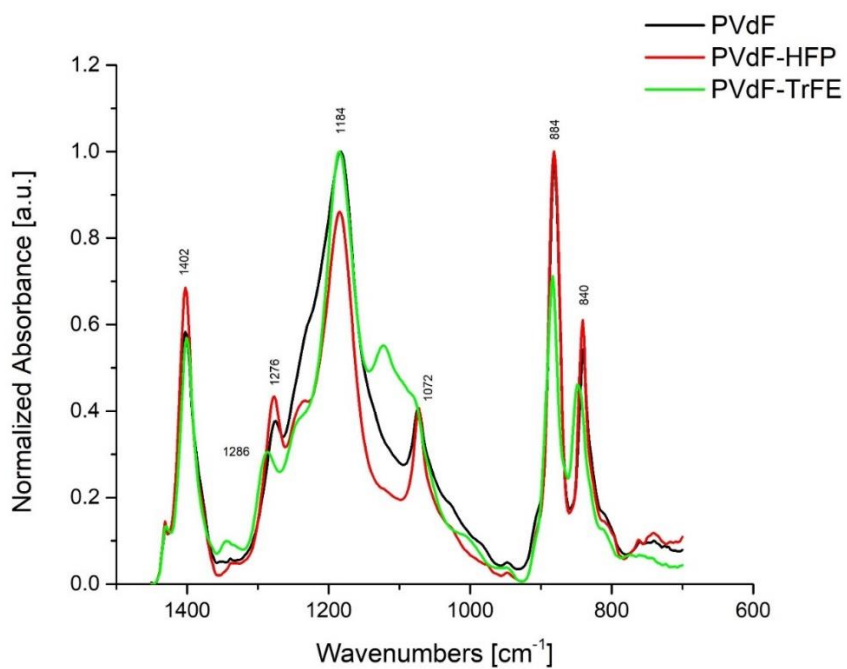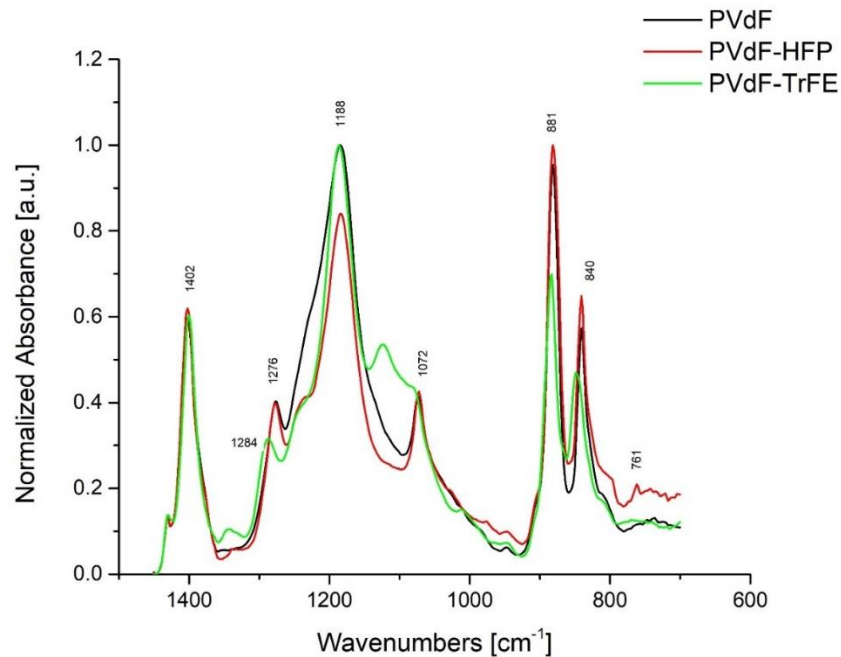(a)   (b)

Figure 30: Diameter distribution for PVDF-TrFE nanomembranes. (a) 2nd year synthesis; (b) 3rd year synthesis


(a)

(b)

Figure 31: FTIR spectra. (a) 2nd year synthesis; (b) 3rd year synthesis

Although the results seem to be better with the optimization process, changes on flow velocity and reducing the shear forces inside the polymeric solutions, as it can be noticed around 761 cm^{-1} wavelength (right side or plot) α phase is present. It means that additional stretching is required to promote an extra α phase β phase transformation. This extra-stretching could be achieved by increasing the electric field or by increasing the polymeric solution electrical conductivity by dispersing carbon nanotubes into the polymeric solution.

During the optimization procedure, 63 nanomembrane samples were synthetized (3 samples for each group). Fourier Transformed Infra-Red analysis were performed in each of one. Figures 32A-C show representative spectra for each group. The addition of carbon nanotubes in three different quantities (small – 0.15 wt. %, medium – 0.30 wt.% , and large – 0.60 wt.%) not only changed nanomembranes' morphology, but it also influenced the piezoelectric activity.

To be able to have apply these nanomembranes as a sensor/actuator the mechanical properties must be determined. Therefore, tensile tests were performed. Figure 33 shows a photo of one nanomembrane during the tensile tests following ASTM D 882 standard. As it can be observed, these nanomembranes are able to support large deformations without breaking. Figures 34A-C show some representative stress-strain curves for the three major groups, PVdF, PVdF-HFP and PVdF-TrFE.
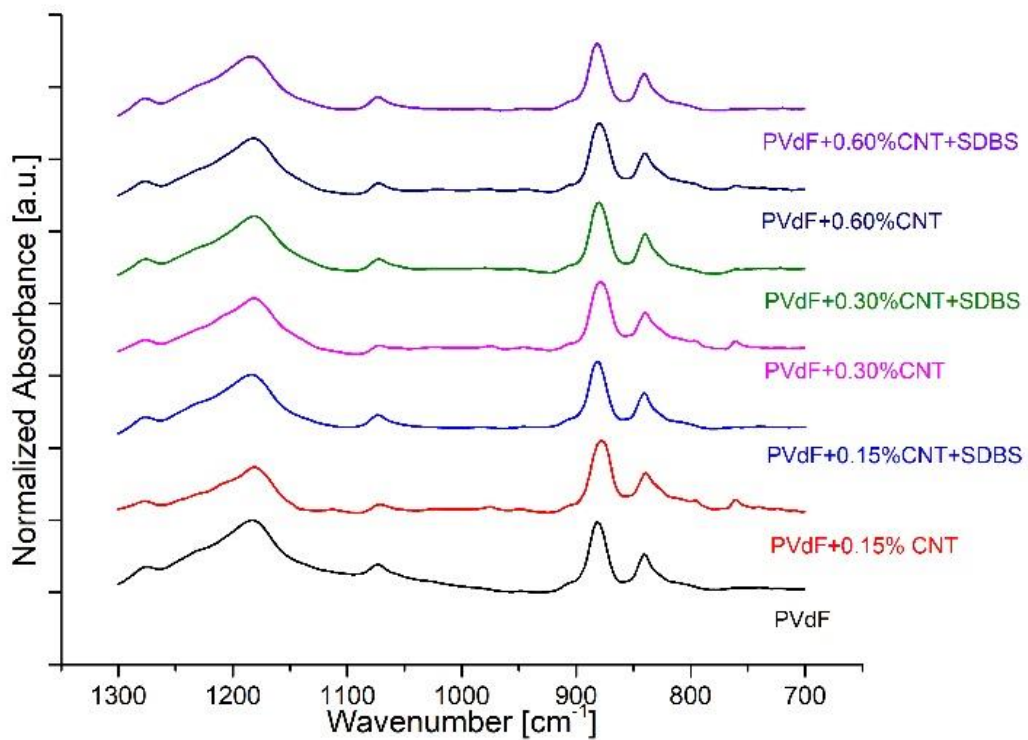
(a)
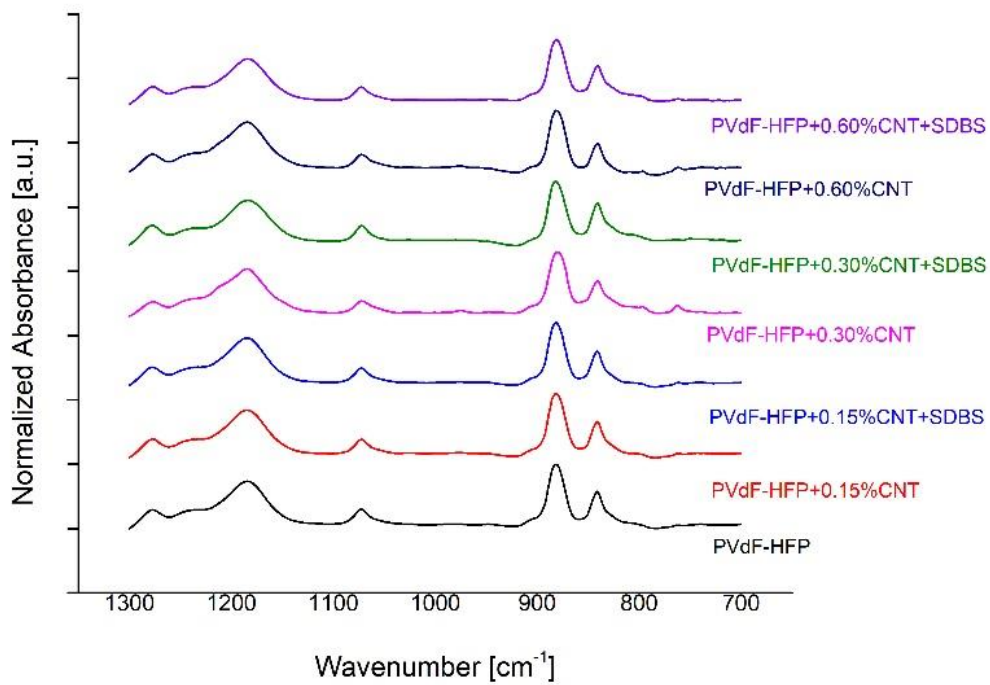
(b)
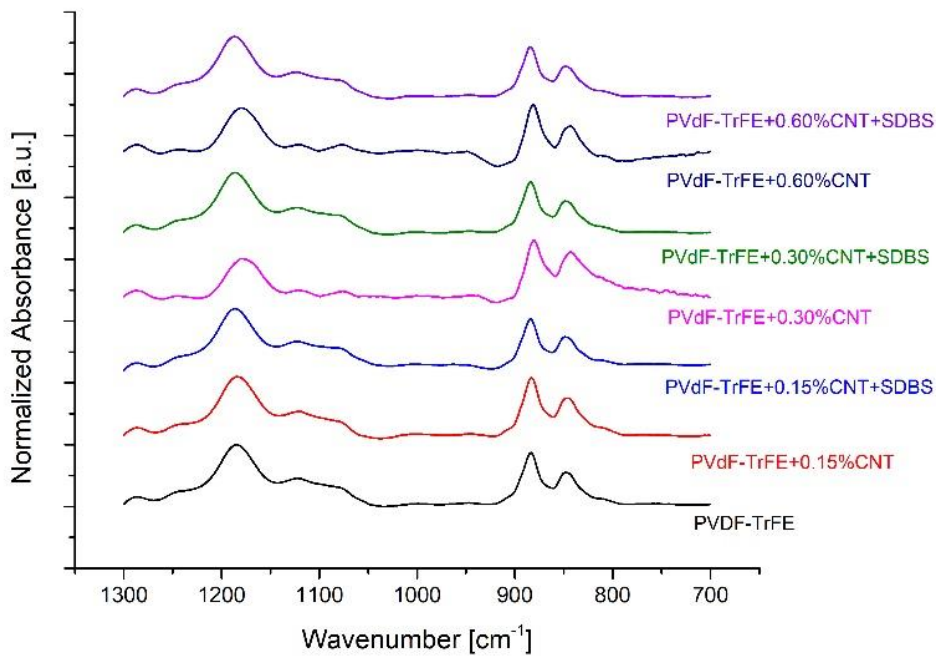
(c)

Figure 32. FTIR Spectra for optimized nanomembranes. (a) PVdF;(b) PVdF-HFP; (c) PVdF-TeFE

Figure 33. Nanomembranes 'deformation during tensile test
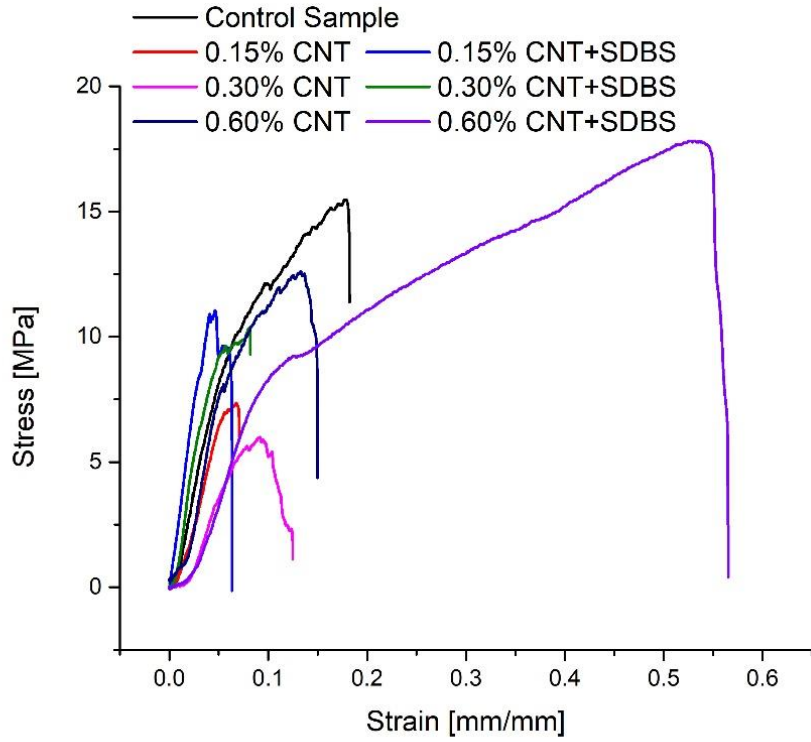
(a)
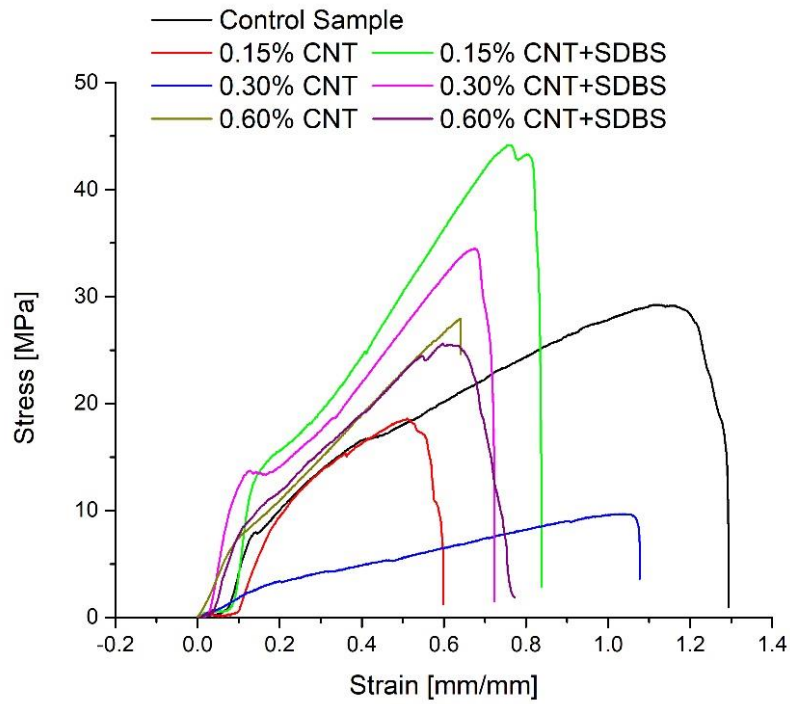
(b)
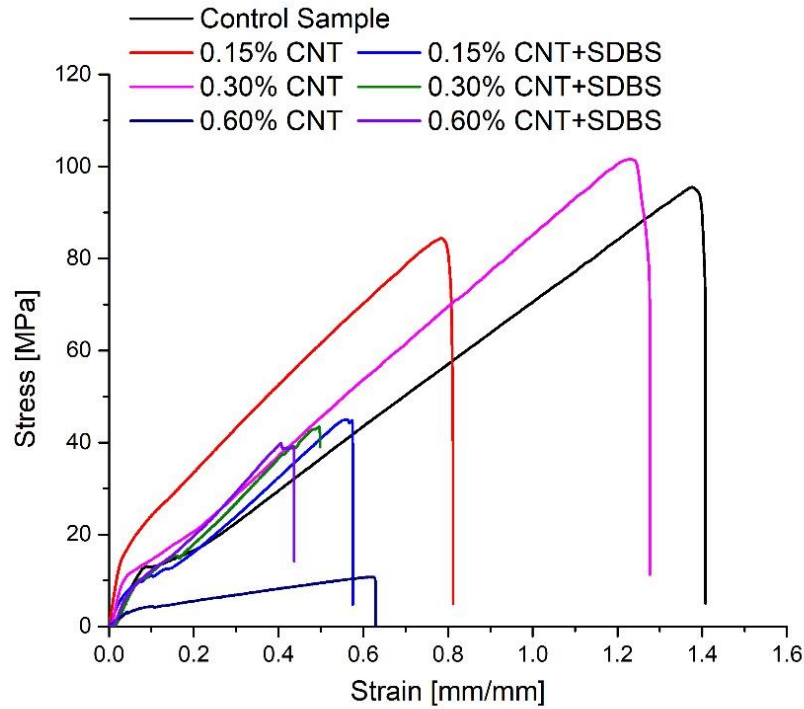
(c)

Figure 34. Stress-Strain curves. (a) PVdF; (b) PVdF-HFP; (c) PVdF-TrFE

Unfortunately, the stress-strain curve variations required an analysis on what was causing this problem. Three sources can be identified, i.e. nanomembranes/fixture misalignment, damage on nanomembranes during the samples preparation and, nanomembranes' anisotropy. A double folded cardboard frame was proposed to some the misalignment problem, while the nanomembranes' anisotropy hypothesis is under evaluation. The second hypothesis was discard as the nanomembranes were removed from the aluminum substrate very easily (see Figure 35). To be able to identify the possibility of anisotropy, tensile tests must be performed with samples prepared at 0 deg, ±45 deg and, 90 deg from the needle's axis.

(a)   (b)
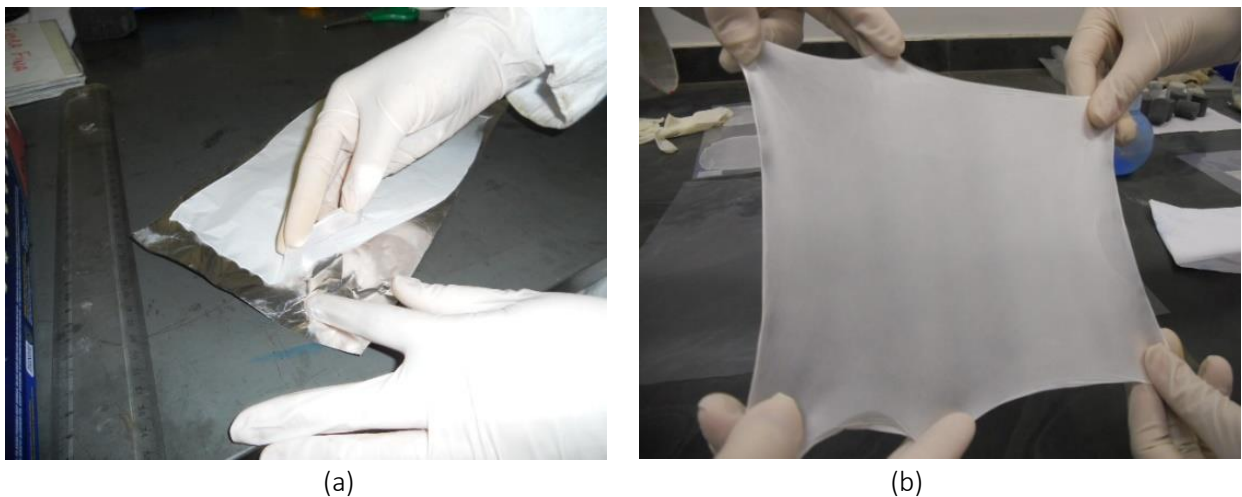
Figure 35. Nanomembrane prepared by electrospinning. (a) Removing from substrate; (b) stretching.

Sensor/actuator design and fabrication:

The sensor/actuator design was based on a combination of PVDF nanomembranes a shape memory alloy (SMA) wires. The concept was explained on the second year report. The first prototype is shown in Figure 36A-C.

(a)

(b)

(c)
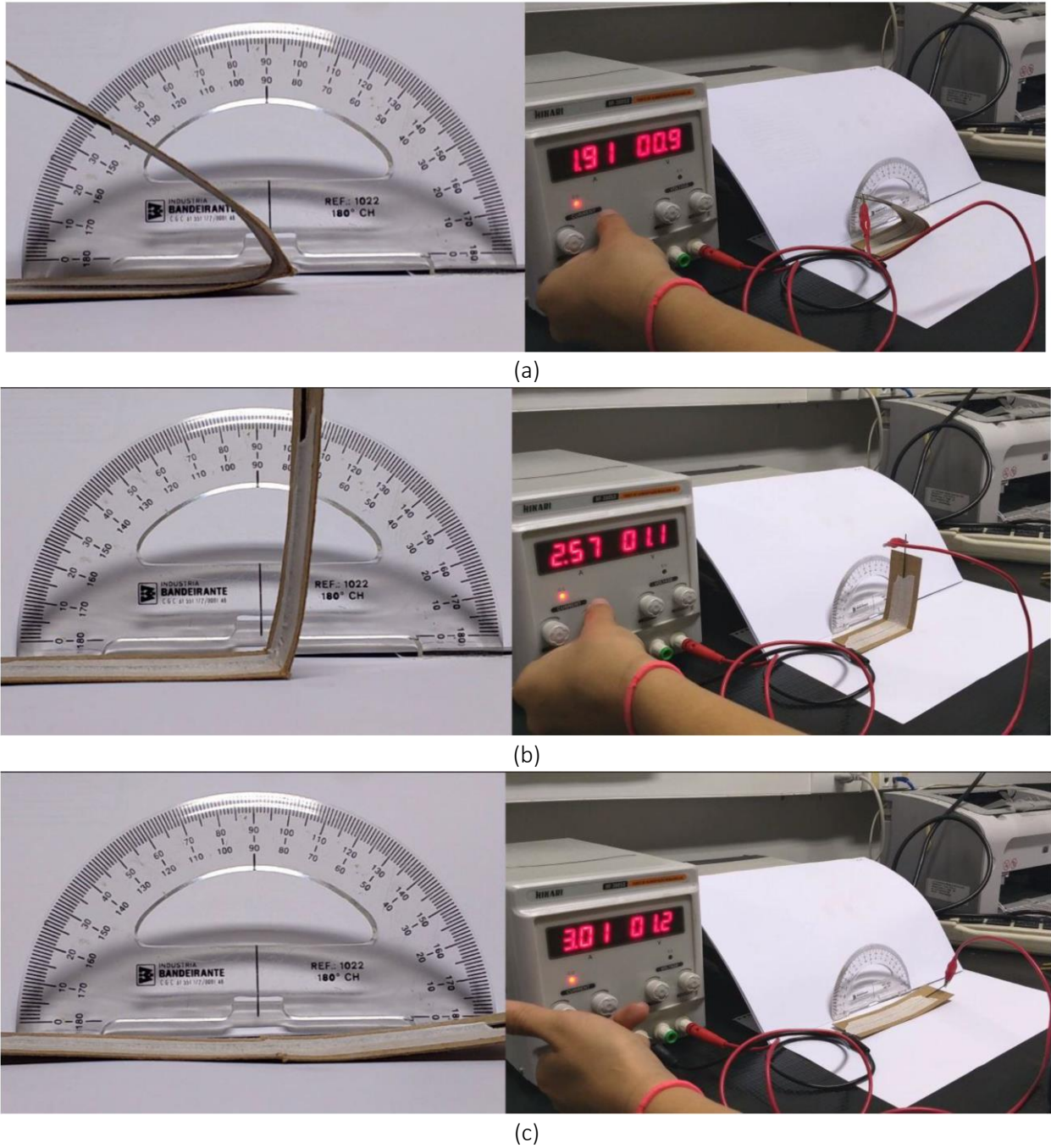
Figure 36. Actuator based on PVDF nanomembranes and SMA wires. (a) Initial position; (b) Intermediate position; (c) final position

The applied voltage was considerably smaller (up to 30 V) than the traditional ones (order of 1000V) and the opening angle ranged from 0 deg to ≈180 deg. The prototype worked but some issues must remain. The force generated by PVDF/SMA system must be quantified. Moreover, the thermal expansion (CTE) mismatch between PVDF and SMA could be a problem. Therefore, a new option is under investigation, i.e. the usage of nanomembranes made of shape memory polymers (SMP). In this investigation, Polycaprolactone (PCL) was selected due to its shape memory characteristics and close CTE.

5.   Publications:

✓ Papers published in Journals:

ÁVILA, ANTONIO FERREIRA; OLIVEIRA, A. M.; LEAO, SUCHILLA G.; MARTINS, M.G. de M.. Aramid Fabric/Nano-size Dual Phase Shear Thickening Fluid Composites Response to Ballistic Impact. COMPOSITES PART A-APPLIED SCIENCE AND MANUFACTURING, v. 112, p. 468-474, 2018

MONTEIRO, ELVIS CARNEIRO; AVILA, ANTONIO FERREIRA . The Carbon Nanotubes Effect into Single-lap Joint Failure Modes and Load Capacity: a Macromechanical Analysis. *Materials Research-Ibero-American Journal of Material* , v.20, p. 143-152, 2018.

LEÃO, SUCHILLA GARCIA ; MARTINS, MARINA GEORGIA DE MELO ; MENEZES, NATHALIA CAROLINE FERREIRA ; LIMA, FERNANDA LUIZA RINCO DE MENDONÇA ; SILVA, CAMILA FERNANDA ; ARANTES, GUILHERME COSTA ; ÁVILA, ANTONIO FERREIRA . Experimental Multi-scale analysis of Carbon/Epoxy Composites Nano-Reinforced by Carbon Nanotubes/Multi-layer Graphene. *Materials Research-Ibero-American Journal of Materials* , v. 20, p. 134-142, 2018.

OLIVA, HENRIQUE N. P. ; AVILA, ANTONIO FERREIRA. Bonded Joints with "Nano-Stitches": Effect of Carbon Nanotubes on Load Capacity and Failure Modes. *Latin American Journal of Solids and Structures* , v. 14, p. 674-684, 2017.

AVILA, ANTONIO FERREIRA.; MUNHOZ, VIVIANE C. ; MENEZES, NATHALIA C. ; SILVA, CAMILA F. DA ; LEIAO, SUCHILLA G. .Non-covalent functionalization of carbon-based nanostructures and its application to carbon/epoxy composites. *International Journal of Nanotechnology* (Online), v. 13, p. 573-583, 2016.

ÁVILA, ANTONIO FERREIRA; OLIVEIRA, A. M.; MUNHOZ, VIVIANE C. ; PEREIRA, G. C. . Graphene-CNTs into Neuron-Synapse Like Configuration a New Class of Hybrid Nanocomposites. ADVANCED MATERIALS RESEARCH (ONLINE), v. 1119, p. 116-120, 2015.

✓ Papers published in Conferences Proceedings:

MONTEIRO, ELVIS ; LEAO, SUCHILLA ; NORTON, MATHEUS; MARTINS, M.G. de M. ; AVILA, ANTONIO F. Fire Behavior of Hybrid Nano-Modified Composites for Airplane Interiors. In: 2018 AIAA/ASCE/AHS/ASC Structures, Structural Dynamics, and Materials Conference, 2018, Kissimmee. 2018 AIAA/ASCE/AHS/ASC Structures, Structural Dynamics, and Materials Conference. Reston: American Institute of Aeronautics and Astronautics, 2018. v. 6.

ÁVILA, ANTONIO FERREIRA.; LIMA, F. C.; MARTINS, M.G. de M.; ARANTES, G. ; NORTON, M. . Modeling Origami-like Structures with near zero Stiffness Modal Analysis and Crease/wrinkle Correlations. In: XXXVIII Ibero-Latin American Congress on Computational Methods in Engineering, 2017, Florianopolis. Proceedings of the XXXVIII Ibero-Latin American Congress on Computational Methods in Engineering. Florianopolis: ABMEC, 2017. v. 37. p. 1-12.

OLIVEIRA, A. M.; LEAO, S. G.; LIMA, F. C.; MARTINS, M.G. de M; ARANTES, G.; NORTON, M.; AVILA, A. F. Nanotechnology for Personal Protection Systems: The New Nano-Modified Bullet Proof Vest Development. In: 24th ABCM International Congress of Mechanical Engineering, 2017, Curitiba. Proceedings of the 24th ABCM International Congress of Mechanical Engineering. Rio de Janeiro: ABCM, 2017. v. 24. p. 1-12.

LEAO, S. G.; LIMA, F. C.; MARTINS, M.G. de M.; MENEZES, N. C. ; NORTON, M.; ÁVILA, A. F. . Mechanics of Hybrid NanoComposites: The Carbon Nanotube/Graphene Effect into Failure Modes. In: 24th ABCM International Congress of Mechanical Engineering, 2017, Curitiba. Proceedings of the 24th ABCM International Congress of Mechanical Engineering. Rio de Janeiro: ABCM, 2017. v. 24. p. 1-12.

LEAO, S. G. ; MENEZES, NATHALIA C. ; LIMA, F. C. ; MARTINS, MARINA GEORGIA DE MELO ; NORTON, M. ; ÁVILA, A. F. . Mechanical Behavior of Piezoelectric Nanomembranes Doped with Carbon Nanotubes. In: 24th ABCM International Congress of Mechanical Engineering, 2017, Curitiba. Proceedings of the 24th ABCM International Congress of Mechanical Engineering. Rio de Janeiro: ABCM, 2017. v. 24. p. 1-10.

MENEZES, NATHALIA C. ; LIMA, F. C. ; SILVA, C. F. ; LEAO, S. G. ; ARANTES, G. ; MARTINS, M. G. ; ÁVILA, A. F. . Carbon Nanotubes Influence on Natural/Synthetic Hybrid Composites Mechanical Properties. In: Thirty-First Technical Conference of the American Society for Composites, 2016, Williamsburg. Proceedings of the Thirty-First Technical Conference of the American Society for Composites. Lancaster: DEStech Publishers, 2016. v. 31. p. 1-12.

AVILA, ANTONIO FERREIRA.; MUNHOZ, VIVIANE C.; OLIVEIRA, ALINE M.; MENEZES, NATHALIA C.; LEAO, SUCHILLA G.; SILVA, CAMILA F. . Non-covalent Functionalization of CNT and Graphene and Its Application to Hybrid Carbon/Epoxy Composites. In: 57th AIAA/ASCE/AHS/ASC Structures, Structural Dynamics, and Materials Conference, 2016, San Diego. 57th AIAA/ASCE/AHS/ASC Structures, Structural Dynamics, and Materials Conference. Reston: American Institute of Aeronautics and Astronautics. v. 57. P.1-10.

ÁVILA, ANTONIO FERREIRA; OLIVEIRA, A. M. ; MUNHOZ, V. C. ; MONTEIRO, E. C. ; PEREIRA, G. C. . Graphene-Carbon Nanotubes Hybrids for Composite Materials. In: AIAA Scitech 2015, 2015, Kissimmee. Proceedings of AIAA Scitech 2015. New York: AIAA, 2015. v. 56. p. 1-12.

OLIVEIRA, A. M. ; MUNHOZ, V. C. ; MONTEIRO, E. C. ; AVILA, A. F. . Thermo-mechanical Analysis of Graphene Based Nanocomposites. In: MecSol 2015 - 5th International Symposium on Solid Mechanics, 2015, Belo Horizonte. Proceedings of the 5th International Symposium on Solid Mechanics. Rio de Janeiro: ABCM, 2015. v. 5. p. 1-8.

SILVA NETO, A.; DIAS, R. A. ; AVILA, ANTONIO F. . New Design to Improve Single-Lap Joint Strength. In: MecSol 2015 - 5th International Symposium on Solid Mechanics, 2015, Belo Horizonte. Proceedings of the 5th International Symposium of Solid Mechanics. Rio de Janeiro: ABCM, 2015. v. 5. p. 1-7.

OLIVA, H. N. P.; FERREIRA, M. M.; ÁVILA, A. F. Study of Adhesive with Hybrid Nanocomposites (CNT and Graphene). In: MecSol 2015 -5th International Symposium on Solid Mechanics, 2015, Belo Horizonte. Proceedings of the 5th International Symposium on Solid Mechanics. Rio de Janeiro: ABCM, 2015. v. 5, p.1-6.

MONTEIRO, E. C.; OLIVEIRA, A. M. ; MUNHOZ, V. C. ; ÁVILA, ANTONIO F. . Multi-Scale Coupling: The Graphene-CNT Carbon Fiber/Epoxy Laminates Investigation. In: MecSol 2015 - 5th International Symposium on Solid Mechanics, 2015, Belo Horizonte. Proceedings of the 5th International Symposium on Solid Mechanics. Rio de Janeiro: ABCM, 2015. v. 5. p. 1-10.

AVILA, ANTONIO F.; MENEZES, N. C. ; CASTAGNA, L. ; SILVA, C. F. ; LIMA, F. C. ; LEAO, S. G. ; FUGER, J. . Bio-Nano-Composites: Flax/Glass-Carbon Laminated Nano-Modified by Carbon Nanotubes. In: Meeting on Aeronautical Composite Materials and Structures - MACMS2015, 2015, Sao Carlos. Proceedings of the Meeting on Aeronautical Composite Materials and Structures. Sao Carlos: USPSC, 2015. v. 1. p. 1-10.

MUNHOZ, V. C.; OLIVEIRA, A. M.; MONTEIRO, E. C. ; ÁVILA, ANTÔNIO FERREIRA . Carbon Based Hybrid Nanostructures for High Performance Composites: The Surfactant investigation. In: 30th Technical Conference of the American Society for Composites, 2015, East Lansing. Proceedings of the 30th Technical Conference of the American Society for Composites. Lancaster PA: DescTech, 2015. v. 30. p. 1-12.

OLIVEIRA, A. M.; MUNHOZ, V. C. ; MONTEIRO, E. C. ; ÁVILA, ANTONIO F. . Nano-Modified Hybrid Recycled Composite: An Alternative for Ballistic Shields. In: 30th Technical Conference of the American Society for Composites, 2015, East Lansing - MI. Proceedings of the 30th Technical Conference of the American Society for Composites. Lancaster - Pa: DEStech, 2015. v. 30. p. 1-12.

OLIVEIRA, A. M. ; MONTEIRO, E. C. ; MUNHOZ, V. C. ; AVILA, ANTONIO F. A New Class for Armor Materials from Recycled Kevlar. In: COBEM 2015 - 23rd International Congress of Mechanical Engineering, 2015, Rio de Janeiro. Proceedings of the 23rd International Congress of Mechanical Engineering - COBEM2015. Rio de Janeiro: ABCM, 2015. v. 23. p. 1-8.

MUNHOZ, V. C.; OLIVEIRA, A. M.; MONTEIRO, E. C. ; Ávila, Antonio F. . Multi-Scale Experimental Analysis of Hybrid Carbon/CNT+Graphene Composites. In: COBEM 2015 - 23rd International Congress of Mechanical Engineering, 2015, Rio de Janeiro. Proceedings of the 23rd International Congress of Mechanical Engineering - COBEM 2015. Rio de Janeiro: ABCM, 2015. v. 23. p. 1-10.

MONTEIRO, E. C.; OLIVEIRA, A. M. ; MUNHOZ, V. C. ; AVILA, ANTONIO F. . The Use of Nano-modified Epoxy Adhesive in Metallic Bonded Joints: Experimental Analysis. In: COBEM 2015 - 23rd international Congress of Mechanical Engineering, 2015, Rio de Janeiro. Proceedings of the 23rd international Congress of Mechanical Engineering - COBEM 2015. Rio de Janeiro: ABCM, 2015. v. 23. p. 1-8.

AVILA, ANTONIO F; CARLEY, G.; GONCALVES, C.. Hybrid Carbon/Epoxy Composites with Interlocking Properties: The Graphene + CNT Nanostructures Morphology Investigation. In: SciTech 2014 AIAA Science and Technology Forum and Exposition, 2014, Washington DC. SciTech 2014 AIAA Science and Technology Forum and Exposition. Washington: AIAA, 2014. p. 1-12.

NASCIMENTO Jr, H.; AVILA, ANTONIO F. Multi-Layer Graphene as Defect Inhibitor to Bonded Joints: The Environmental Effects Investigation. In: 29th American Composite Society Technical Conference, 2014,

San Diego. Proceedings of the 29 ASC Technical Conference. Lancaster, PA: DEStech Publishers, 2014. v. 29. p. 1-12.

CARLEY, G.; AVILA, ANTONIO F. A Synergetic Coupling between Graphene and Carbon Nanotubes for Hybrid Carbon Fiber Composites. In: 29th American Composite Society Technical Conference, 2014, San Diego. Proceedings of the 29 ASC Technical Conference. Lancaster, PA: DEStech Publishers, 2014. v. 29. p. 1-16.

MUNHOZ, V.; OLIVEIRA, A. M.; AVILA, ANTONIO F Polymeric Nano-Coatings with Super-hydrophobic Properties. In: XIV Latin American Symposium on Polymers and XII Latin American Congress on Polymers, 2014, Porto de Galinhas. Proceedings of the XIV Latin American Symposium on Polymers and XII Latin American Congress on Polymers. Sao Paulo: ABPOL, 2014. v. 14. p. 1-5.

OLIVEIRA, A. M.; MUNHOZ, V.; AVILA, ANTONIO F. Tailoring Nanomembrane Morphology and Surface Tension: The Self-Cleaning Coating. In: XIV Latin American Symposium on Polymers and XII Latin American Congress on Polymers, 2014, Porto de Galinhas. Proceedings of the XIV Latin American Symposium on Polymers and XII Latin American Congress on Polymers. Sao Paulo: ABPOL, 2014. v. 14. p. 1-5.

AVILA, ANTONIO F.; MUNHOZ, V. C.; OLIVEIRA, A. M.; PEREIRA, G. C. Graphene-CNTs into Neuron-Synapse-Like Configuration a New Class of Hybrid NanoComposites. In: 2014 International Conference on Nanotechnology and Biosensors (ICNB 2014), 2014, Barcelona. Proceedings of the 2014 International Conference on Nanotechnology and Biosensors (ICNB2014). Beijing: IACSIT, 2014. v. 5. p. 1-5.

.